Review

Recent Progress in Multiphase Thermoelectric Materials

Raphael Fortulan [1] and Sima Aminorroaya Yamini [1,2,*]

1   Materials and Engineering Research Institute, Sheffield Hallam University, Sheffield S1 1 WB, UK; b9044884@my.shu.ac.uk
2   Department of Engineering and Mathematics, Sheffield Hallam University, Sheffield S1 1 WB, UK
*   Correspondence: s.aminorroaya@shu.ac.uk

Abstract: Thermoelectric materials, which directly convert thermal energy to electricity and vice versa, are considered a viable source of renewable energy. However, the enhancement of conversion efficiency in these materials is very challenging. Recently, multiphase thermoelectric materials have presented themselves as the most promising materials to achieve higher thermoelectric efficiencies than single-phase compounds. These materials provide higher degrees of freedom to design new compounds and adopt new approaches to enhance the electronic transport properties of thermoelectric materials. Here, we have summarised the current developments in multiphase thermoelectric materials, exploiting the beneficial effects of secondary phases, and reviewed the principal mechanisms explaining the enhanced conversion efficiency in these materials. This includes energy filtering, modulation doping, phonon scattering, and magnetic effects. This work assists researchers to design new high-performance thermoelectric materials by providing common concepts.

Keywords: thermoelectric materials; multiphase; composite; energy filtering; magnetic effect; phonon scattering

1. Introduction

Thermoelectric (TE) materials have been attracting a great deal of interest because of their applications in energy recovery from industrial waste heat and high-efficiency cooling of next-generation integrated circuits [1]. The efficiency of TE materials is characterised by a dimensionless figure of merit $zT = S^2\sigma T/(\kappa_e + \kappa_l)$, where T, S, σ, κ_e and κ_l are the absolute temperature, Seebeck coefficient, electrical conductivity, and electronic and lattice components of the total thermal conductivity (κ_t), respectively. Most thermoelectric materials used in commercial applications have a zT of around 1 [2], which corresponds to an efficiency of roughly 10% in the medium temperature range [3]. To increase zT, one would need to increase S and σ and decrease κ_t. These parameters are interrelated though; the electronic thermal conductivity increases with the increase of electrical conductivity, and S and σ are inversely proportional [4]. Therefore, optimising these parameters is very challenging and the key to achieving higher efficiency.

One of the most successful approaches to improve the figure of merit is reducing the lattice thermal conductivity, and over the years, various phonon engineering approaches have been used to enhance phonon scattering and decrease κ_l by taking advantage of nanoprecipitates [5–7], alloying elements [8–10], nanostructured grain boundaries [11–14], ionised impurities [15,16], and superlattices [17].

A series of band structure engineering approaches have also been employed to improve the electronic properties [18–20]. Strategies such as quantum confinement [21,22], modulation doping [23–25], introducing resonance energy to the electronic density of states [26,27], and energy filtering [28] are being actively pursued. These strategies are adopted to modify the band structure and transport properties of the thermoelectric materials by either tuning the electrical conductivity and the Seebeck coefficient independently or by increasing them simultaneously. In practice, the best results were achieved with a

significant increase in one of these parameters and a slight decrease in the other, resulting in an increase in the power factor ($S^2\sigma$) and zT.

The development of highly efficient thermoelectric materials encountered a bottleneck when the exploration of single-phase alloys was exhausted. Therefore, investigating multiphase compounds is the most viable strategy to enhance the thermoelectric performance of bulk materials, where higher degrees of freedom are available to design new materials and tune their electronic transport properties [29–31]. Figure 1 presents the number of yearly publications on thermoelectric materials, indexed by the Scopus database, compared with the numbers of papers published on multiphase/composite thermoelectric materials, indicating an increasing interest of the research community on this topic over the last five years.
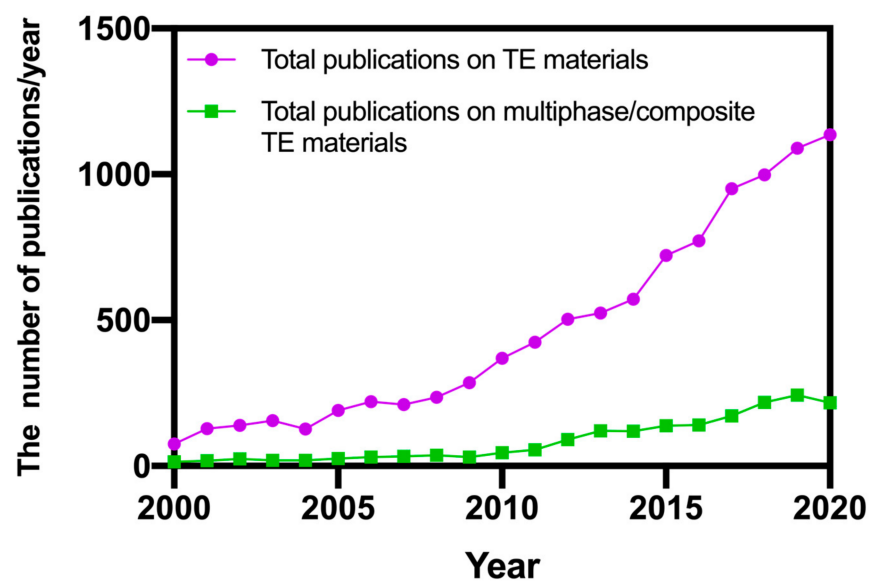
Figure 1. Yearly number of publications on thermoelectric materials, compared with publications on multiphase/composite thermoelectric materials.

The combination of several phases can improve the electrical conductivity, Seebeck coefficient, and thermal conductivity [32]. Here, we summarise the main strategies discovered to date to increase the thermoelectric efficiency in multiphase materials. This includes: (1) energy filtering, creating potential barriers in the electronic band structure of the main phase through interfaces with the secondary phases. This results in an increase in the overall Seebeck coefficient [33–35]; (2) modulation doping, where the heterojunctions between secondary phases with larger bandgaps and higher carrier concentrations than the matrix are used to greatly increase the electrical conductivity of the multiphase compounds [36–38]; (3) phonon scattering by interfaces, grain boundaries, and defects to reduce the lattice thermal conductivity [39–42]; and (4) magnetic effects, which utilises the magnon-drag mechanism in magnetic materials [43–45], semiconductors doped with magnetic elements [46–48], or semiconductors containing secondary magnetic phases [49,50] to improve the thermoelectric efficiency [51,52].

2. Energy Filtering

The concept of energy filtering in thermoelectric materials was first introduced and studied in the latter half of the last century [53]. The research on this field has been renewed and developed since the 1990s. In general, the Seebeck coefficient increases with an increase of the barrier height [54,55] while the electrical conductivity decreases [56–58]. In the presence of multiple potential barriers, the bipolar effect can be suppressed, decreasing the flow of minority charge carriers and reducing the decrease in the electrical conductivity [59–62].

Conventionally, the energy filtering effect could be understood by solving the Boltzmann transport equation (BTE) using the relaxation time approximation [63,64]. The BTE equation expresses all thermoelectric transport coefficients as a function of the energy-dependent relaxation times of the charge carriers $\tau(E)$ and the Fermi level E_F. The energy filtering effect can be readily verified considering the Seebeck coefficient expression [65]:

$$S = -\frac{1}{qT} \frac{\int (E - E_F)\sigma'(E)\mathrm{d}E}{\int \sigma'(E)\mathrm{d}E} \tag{1}$$

where T is the absolute temperature, E is the charge carrier energy, E_F is the Fermi level, and σ' is the differential conductivity. The Seebeck coefficient, as shown in Equation (1), is the energy average weighted by the electrical conductivity:

$$S = -\frac{1}{qT} \langle E - E_F \rangle_{\sigma'} \tag{2}$$

implying that an asymmetry between the density of states and the Fermi level can create higher Seebeck coefficients.

The implementation of energy barriers in thermoelectric materials is made in the form of either nanoparticles or grain boundary interfaces embedded in the bulk host matrix [66]. At these interfaces, the carriers with higher energy will pass the interface preferentially, while the carriers with lower energy are filtered out. A high density of the interfaces ensures the positive carrier filtering effect [67]. The band bending between the two materials creates an energy barrier that reflects the charge carrier [68,69]. Figure 2 illustrates the energy filtering effect: given the partial reflection of the lower energy electron waves, the high energy electrons mostly contribute to the Seebeck coefficient.
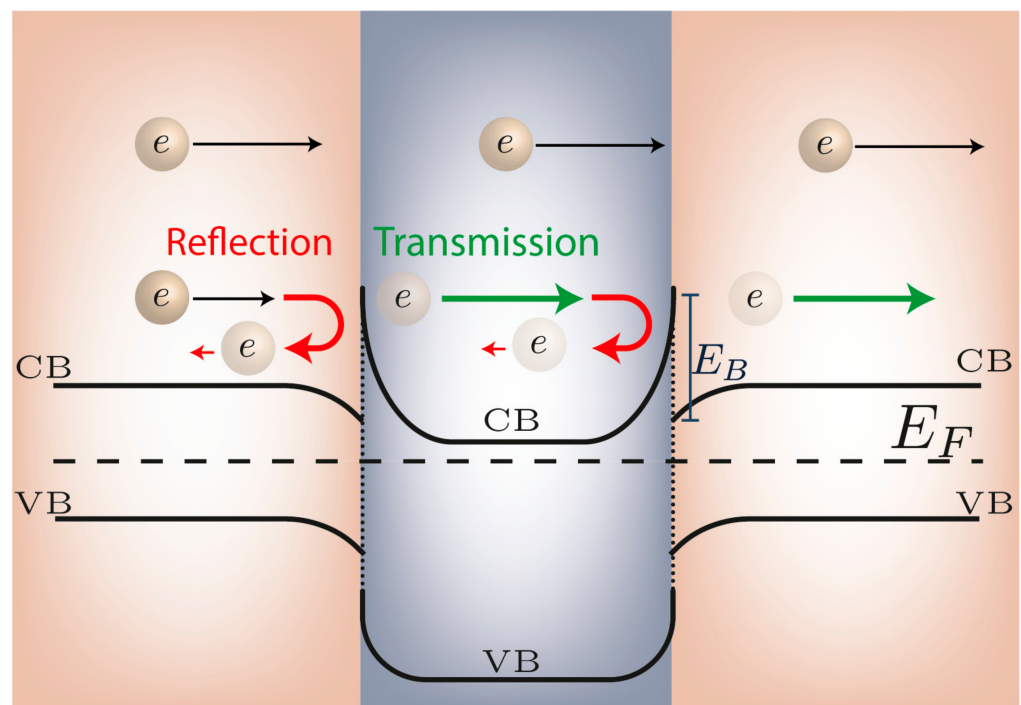
Figure 2. Energy filtering effect, showing that lower energy electrons are scattered by a potential barrier.

Multiphase materials present themselves as viable candidates to take advantage of energy filtering. Given the possibilities of tuning the electronic band structure of each phase, the band bending can noticeably enhance the energy filtering effect [70–77]. In the following sections, the energy filtering effect will be discussed in multiphase materials. A Schottky or ohmic barrier will appear at the interface with a metallic secondary phase,

while a heterojunction barrier will present at the interface of thermoelectric material with a semiconducting secondary phase.

2.1. Energy Filtering by Metal Secondary Phases

For metallic phases, the barrier height will be proportional to the work function of both the semiconductor and the metal and the electron affinity of the semiconductor. The work function, Φ, is defined as the minimum energy required to remove an electron from the surface of a material, and its value is equal to the energy difference between the vacuum and the Fermi level [78]. The electron affinity, χ, is the energy difference between the vacuum and the bottom of the conduction band. At the metal–semiconductor junction, the Schottky-Mott rule [79] defines the barrier height, E_B, to be the difference between the metals' work function, Φ_M, and the semiconductor electron affinity, χ_S:

$$E_B = \Phi_M - \chi_s \tag{3}$$

Small differences cause few restrictions on the movement of the electrons, and this barrier is known as ohmic. Both the work function and electron affinity depend on the surface impurity and the crystallographic orientation.

Theoretically, the presence of metals can strongly affect the carrier relaxation time and consequently affects both the electrical conductivity and the Seebeck coefficient [54,80,81]. The inclusion of metallic nanoparticles was shown to enhance the Seebeck coefficient mathematically [66]. The interface of *n*-type PbTe with metallic Pb nanoparticles, with a low work function, effectively scattered the electrons and increased both the Seebeck coefficient and electrical resistivity. This mechanism is illustrated schematically in Figure 3, where spherical metallic nanoparticles are randomly distributed in a host semiconductor.
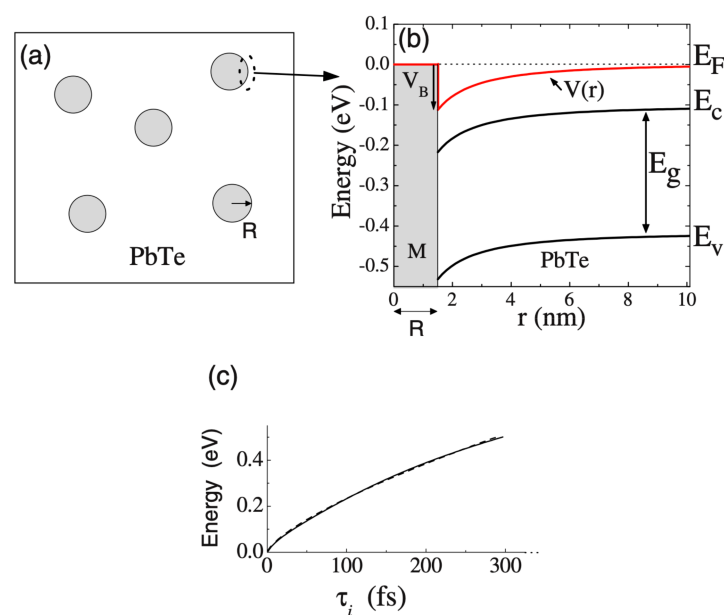
Figure 3. (**a**) Schematic of randomly distributed metallic Pb secondary phase in a PbTe matrix (**b**) Calculated potential V(r) and energy diagram for PbTe at 300 K, carrier concentration of 2.5×10^{19} cm^{-3}, barrier height of 0.11 eV, and radius of 1.5 nm, where E_F is the Fermi level, E_C is the energy at the bottom of the conduction band, E_g is the band gap, and E_V is the energy at the top of the valence band (**c**) Carriers' relaxation time as a function of their energy. Reprinted with permission from ref. [66]. Copyright 2008 Copyright American Physical Society.

Experimental results have proved this concept [82–84]: for instance, Pb precipitates in the matrix of *n*-type PbTe, intrinsically doped with excess Pb, increased the Seebeck coefficient and the average resistivity from -98 µV/K and 1.2 mΩ cm for Pb$_{1.03}$Te to

-130 µV/K, and 3.2 mΩ cm for $Pb_{1.06}Te$ at 300 K, respectively [82]. The addition of metallic Sn and Cr to Cu_2O doubled the Seebeck coefficient from 700 µV/K to 1400 µV/K [84]. Platinum nanocrystals created energy barriers in *p*-type Sb_2T_3 thin films [83] and caused a large reduction in carrier mobility in about 2.5 orders of magnitude due to the additional scattering of charge carriers compared to Sb_2Te_3 films without Pt nanocrystals. The carrier concentration increased, possibly due to the overlapping of energy bands [66]. The band overlapping increases the distance between the Fermi energy level and the valence band maxima, thereby increasing the total concentration of holes in the semiconductor matrix.

Silver nanoparticles enhanced the Seebeck coefficient of CdO-Ag composites [85]—a potential barrier of $E_B = 0.1$ eV between the work function of Ag and the electron affinity of CdO increased the resistivity from 1.5 mΩ cm to 1.7 mΩ cm for a sample with 0.03% of Ag and increased the Seebeck coefficient from -120 µV/K for the pristine sample to -129 µV/K for the sample with 0.03% of Ag at 800 K.

2.2. Energy Filtering by Semiconducting Secondary Phases

For a semiconductor secondary phase, the difference between the bandgaps and Fermi levels of the two phases gives rise to a potential barrier at their junction [86]. The barrier height will be proportional to the difference between the electron affinity of the two semiconductors (χ_1, χ_2). Anderson's rule [78] allows a simple estimate of the barrier height at the conduction, E_{BC}, and valence, E_{BV}, bands:

$$E_{BC} = \chi_2 - \chi_1 \tag{4}$$

$$E_{BV} = \left(E_{g1} - E_{g2} \right) - E_{BC} \tag{5}$$

and it has been employed as a rough estimation to design multiphase materials. The actual curvature of the band bending can be found using Poisson's equation for the electric potential [87]:

$$-\nabla^2 V = \frac{\rho}{\varepsilon} = \frac{q(h - n + D)}{\varepsilon} \tag{6}$$

where ε is the permittivity of the material, h and n are the holes and electrons densities, respectively, and D is the concentration of ionised impurities (extrinsic dopant). The relation of the barrier height and conductivity is suggested as [88]:

$$\sigma \propto T^{-\frac{1}{2}} e^{-\frac{E_B}{k_B T}} \tag{7}$$

It should be noted that this equation was developed for homojunctions [89,90]. However, experimental data for heterojunctions fit this equation surprisingly well [91]. Experimental results show that energy filtering caused by dissimilar semiconducting phases can improve the power factor [92–95]. Silicon oxide particles in the $(Bi_2Te_3)_{0.2}(Sb_2Te_3)_{0.8}$ bulk alloy increased the Seebeck coefficient from 182 µV/K for the pristine sample to 218 µV/K for the sample with 1.1% volume of SiO_2 at room temperature [92]. Yttrium oxide (Y_2O_3) particles embedded in a $Bi_{0.5}Sb_{1.5}Te_3$ matrix increased the Seebeck coefficient significantly [96], deviated considerably from the ideal Pisarenko relation. The Seebeck coefficient is inversely proportional to the carrier concentration, *n*, by a rate of $n^{-2/3}$ for degenerate semiconductors, according to the Pisarenko relation [97]. The deviation from this ideal relationship has been used as an indication of changes in the electronic band structure of the material [98].

Randomly dispersed titanium dioxide nanoparticles (ranging from 10 to 25 nm) in a $Ba_{0.22}Co_4Sb_{12}$ matrix increased the Seebeck coefficient [99]. Although the bandgap for $Ba_{0.22}Co_4Sb_{12}$ was unknown, given the large bandgap of TiO_2 (3.2 eV [100]), some influence of the energy filtering was assumed. At 300 K, the electrical conductivity decreased from 2.9×10^5 S/K to 2.8×10^5 S/K, and the Seebeck coefficient increased from -105 µV/K for the pristine sample to -110 µV/K for the sample with 0.8% volume of TiO_2. The TiO_2 particles in Bi_2Se_3 based materials increased the overall power factor of the composite

from 0.75×10^{-3} W/m K to 1.07×10^{-3} W/m K for the sample with 10 wt.% of titanium dioxide [101]. The charge carrier concentration varied greatly with the concentration of TiO_2, possibly due to the formation of Ti^{2+} ions during hot pressing under the vacuum.

Interestingly, a double-filtering effect has been reported for a deposited TiO_2 on $TiC_{1-x}O_x@TiO_y$ ($x < 1$, $1 < y < 2$) heterostructures (Figure 4) [102]. $TiC_{1-x}O_x$, with a narrow bandgap and high electrical conductivity, in combination with TiO_y and TiO_2 nanoparticles, with wide bandgaps, produced an effective barrier height for energy filtering. The Seebeck coefficient and resistivity of the samples increased where a larger amount of TiO_2 was deposited. The maximum value obtained for the Seebeck coefficient at 973 K was -156 µV/K, with an electrical conductivity of ~4×10^4 S/m.
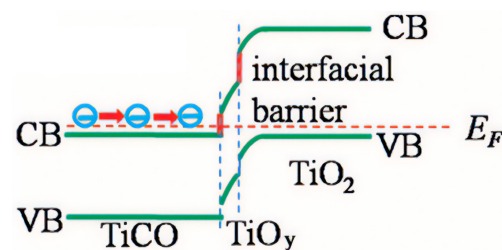
Figure 4. Band diagrams of the $TiC_{1-x}O_x@TiO_y$-TiO_2 heterostructured interface, where CB is the conduction band, VB is the valence band, and E_F is the Fermi level. Reprinted from [102].

Silicon-based materials, although not common in thermoelectricity, have also been shown to benefit from energy filtering [103–110]. For instance, heavily doped Si with B with nanoparticles of Si has shown an increased Seebeck coefficient and electrical conductivity in a particular range of dopant concentrations [111]. The increased Fermi level for the bulk material explains the increase of the electrical conductivity, and the energy filtering effect justifies the increased Seebeck coefficient.

A half-Heusler compound of $(Hf_{0.6}Zr_{0.4})NiSn_{0.99}Sb_{0.01}$, with added nanoparticles of tungsten (W), showed a maximum zT of 1.4 at 873 K and average zT of 0.9 in the temperature range of 300–973 K for the alloy with 5 wt.% tungsten nanoparticles [112].

Table 1 summarises the compositions and fabrication methods of recent studies that reported energy filtering effects in multiphase thermoelectric materials.

Table 1. Compositions, fabrication methods, and corresponding references of multiphase materials that benefited from the energy-filtering effect.

Composition	Fabrication Technique	Ref.
$Bi_{0.5}Sb_{1.5}Te$ + (0, 1.0, 2.0, 4.0, and 6.0 wt.%) nanoparticles of Sb_2O_3	Casting ($Bi_{0.5}Sb_{1.5}Te$) + ball milling of $Bi_{0.5}Sb_{1.5}Te$ and commercial powder of Sb_2O_3+ sintering	[113]
$Bi_2Te_{2.7}Se_{0.3}$ powder + ~2 nm layer of film of ZnO	Solution-based synthesis of Bi-Te-Se powder + atomic layer deposition of ZnO + hot pressing	[114]
$Bi_{1-x}Sb_x$ (x = 0, 0.10, 0.12, 0.13, 0.14, 0.2) + 3 wt.% carbon nanotubes	Ball milling + cold pressing + annealing	[115]
$Bi_{0.46}Sb_{1.54}Te_3$ + (0, 0.1, 0.2, and 0.3 wt.%) SiC	Ball milling + sintering	[70]
$Bi_{0.4}Sb_{1.6}Te_3$ + (0.1%, 0.2%, and 0.3 wt.%) $CuInTe_2$	Casting each phase separately + ball milling + sintering	[116]
$Lu_{0.1}Bi_{1.9}Te_3$ + (0, 0.0, 0.05, 1) wt.% carbon nanotubes	Hydrothermal synthesis + grinding + hot pressing	[117]
$Bi_{0.5}Sb_{1.5}Te_3$ + (0, 0.1, 0.2, 0.3, 0.4 wt.%) $BaTiO_3$	Hydrothermally synthesised $BaTiO_3$ + Commercial ingots of $Bi_{0.5}Sb_{1.5}Te_3$ were grinded and sintered	[74]
$Bi_{0.5}Sb_{1.5}Te_3$ + $SrTiO_3$	$Bi_{0.5}Sb_{1.5}Te_3$ films were grown on $SrTiO_3$ substrates by co-sputtering	[118]
Bi_2Te_3 + $Bi_{0.5}Sb_{1.5}Te_3$ thin films	Radio-frequency magnetron sputtering of Bi_2Te_3/$Bi_{0.5}Sb_{1.5}Te_3$ layers on a SiO_2/Si(001) substrate	[119]
$Bi_{0.4}Sb_{1.6}Te_3$ + (0, 0.2, 0.4, and 0.6 vol.%) $CuGaTe_2$	Vacuum melting + hot pressing	[120]
$Bi_{0.5}Sb_{1.5}Te_3$ + 2 wt.% (Gd_2O_3, $Gd_{1.98}Bi_{0.02}O_3$)	Powders for each phase were prepared by induction melting then mixed by spray pyrolysis + sintering	[121]
Bi_2Te_3 + (1, 2, and 5 wt.%) SnS	Commercial powders were mixed, cold pressed, and annealed	[122]
$Bi_{0.3}Sb_{1.7}Te_3$ + (0, 0.25, 0.50, and 0.75 wt.%) TiC	Ball milling + sintering	[123]
Bi_2Te_3 + ~4 wt.% of $Cu_{1.5}Te$	Solution-based synthesis (each phase separately) + hot pressing	[124]

Table 1. *Cont.*

Composition	Fabrication Technique	Ref.
Coated grains of SnTe with CuInTe$_2$	CuInTe$_2$ was formed by cation exchange of Sn by Cu and In on the surface of ball-milled SnTe powder	[125]
Bi$_{0.5}$Sb$_{1.5}$Te$_3$-Cu$_{0.07}$ + (0, 0.5, and 1.0 wt.%) HfO$_2$	Water atomisation + ball milling + sintering	[126]
SiGe + (2, 4, 6, 8, 10 wt.%) TiB$_2$	Ball milling + hot pressing	[108]

3. Modulation Doping

Modulation doping is a well-recognised concept to increase the conductivity in heterojunction devices [127]. The main idea behind modulation doping is to use the offset in the band structure between two semiconductors in combination with heavy doping of the material with a wider bandgap so that there is a transfer of carriers from the wide bandgap to the narrow bandgap material. The transferred carriers create two-dimensional electron gas, and they are essentially separated from the donor phase, which consequently increases the charge carrier mobility [128]. Conventionally, this strategy was employed to create *p*-channel devices, called modulation-doped field-effect transistors (MODFET) [129]. The difference between energy filtering and modulated doped samples is shown schematically in Figure 5. In the case of modulation doping, the secondary phase increases the conductivity by donating electrons to the host semiconductor, while in the case of energy filtering, the secondary phase scatters electrons and reduces mobility.
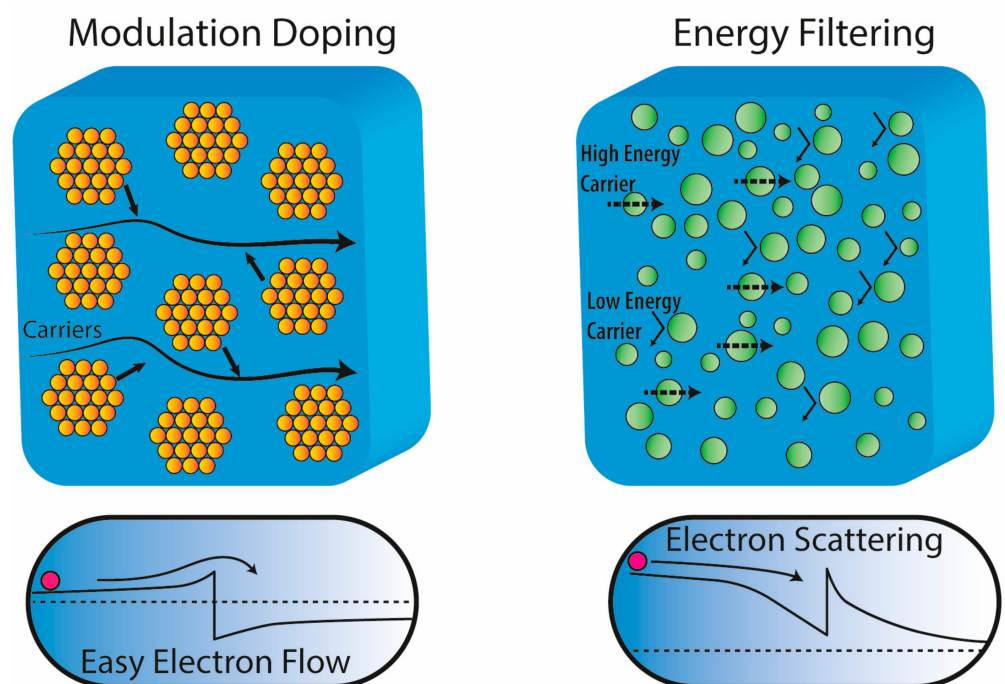
Figure 5. Comparison between a modulated doped semiconductor and a multiphase compound benefiting from energy filtering.

The thermoelectric research community has also used this mechanism to enhance the thermoelectric performance of materials [15,23,25,29,38]. For thermoelectric materials, a combination of two effects has enhanced the thermoelectric efficiency in the modulated doped materials: firstly, a large increase in the electrical conductivity and mobility of the charge carriers [130], and secondly, a reduction in the lattice thermal conductivity as a result of the scattering of phonons by nanostructuring [23,131].

Some attempts have also been made to explore the possibility of using modulation doping in structures similar to field-effect transistors (FETs) [129]. In this adopted structure,

the thermoelectric semiconductor nanowire (channel) is enclosed by the heavily doped layer (gate) [132–136]. A modest increase in the power factor was achieved by this approach.

Table 2 summarises the sample compositions, fabrication methods, and corresponding references of recent studies that employed modulation doping to enhance the thermoelectric performance of multiphase materials.

Table 2. Sample compositions and fabrication methods of references that employed modulation doping to enhance the thermoelectric performance of multiphase materials.

Composition	Fabrication Method	Ref.
$Ba_8(Al_xGa_{1-x})_{16}Ge_{30}$ (x = 0, 0.20, 0.23, 0.25, 0.33, 0.50, and 1)	Casting (each phase separately) + ball milling + sintering	[137]
$AgBiSe_2$ + Bi_4Se_3		[138]
Cu_2SnS_3 + (0, 1, 3, and 5% mol) $CuCo_2S_4$	Casting (each phase separately) + ball milling + sintering	[25,139]
$Si_a(Mg_2Si + x$ at. % $Bi)_{1-a}$ (a = 0.39, 0.50, 0.56, 0.59, and 0.67; x = 0.3, 0.8, 1.3, 1.8, 2.5)	Bi-doped Mg_2Si fabricated using induction melting + melt spinning si + sintering	[140]
p-type organic conducting polymer PEDOT:PSS + Ge	PEDOT:PSS coated with Ge layer	[141]
$(Ge_2Te_2)_x(CuInTe_2)_{1-x}$ (x = 98, 95, 90, 87.5, 85, 70, 30, and 10%)	Casting + hand milling + hot pressing	[142]
$BiCuSeO$ + $Bi_{0.8}Pb_{0.2}Cu_{0.8}Ni_{0.2}SeO$	Each phase was fabricated by Mechanical alloying + ball milling of mixture + sintering	[143]
$BiCuSeO$ + $Bi_{0.8}Er_{0.2}CuSeO$	Each phase was fabricated by ball milling + sintering. The final composition was obtained by ball milling + sintering	[144]
$BiCuSeO$ + $Bi_{0.8}Ba_{0.2}CuSe_{0.8}Te_{0.2}O$	Each phase was fabricated by mechanical alloying + milling the mixture + sintering	[145]
$Pb_{(1-x)}Na_xTe_{0.65}S_{0.25}Se_{0.1}$ (x = 0.005, 0.01, 0.0015, 0.02, 0.025, and 0.03)	Casting PbSe and PbS + mixing stoichiometric amounts of PbSe, PbS, Pb, Te, and Na (casting) + sintering	[29]
$Pb_{0.97}Na_{0.03}Te_{(1-x)}S_x$ (x = 0.1, 0.15, 0.2, 0.25, 0.3, and 0.35)	Casting + hand milling + sintering	[146]

4. Phonon Scattering

When it comes to designing a thermoelectric material, the main goal is to maintain a high electrical conductivity while, at the same time, reduce the thermal conductivity to reach an amorphous solid [147]. In semiconductors, phonon transport plays a significant role in thermal conductivity [148,149]. Increasing phonon scattering has, therefore, proven to be a key strategy to improve the efficiency of thermoelectric materials [150]. This is mainly performed by nanostructuring of the material [151], introducing grains with sizes larger than the mean free path of the charge carriers but smaller than the mean free path of the phonons [152], alloy scattering with additional mass or strain fluctuation [153–155], nanocomposites [156–159], and embedding interfaces by creating texture between the two materials [160].

In thermoelectric materials, the phonon-scattering mechanisms are assessed using models for the total thermal conductivity. Traditional models are from Klemens [161], Holland [162], and Callaway [163]. Impurity scattering, boundary scattering, three-phonon normal process, and Umklapp process are considered in these models, and Matthiessen's rule is employed to determine the overall relaxation time.

The Klemens model has been successfully used to evaluate the contribution of each phase on the lattice thermal conductivity [164,165]. In this model, the thermal conductivity for each type of scattering mechanism is evaluated independently, and the overall thermal conductivity is given by [161]:

$$\kappa_{tot}^{-1} = \sum_i \kappa_i^{-1} \tag{8}$$

For phonon-point defects, the relaxation time is given by [161]:

$$\tau_I = \frac{\Gamma V}{4\pi \nu_s^3} \omega^4 \tag{9}$$

where ν_s is the average sound speed on the material, V is the average atomic volume, and Γ is the mass-fluctuation, phonon-scattering parameter [166]:

$$\Gamma = \frac{\overline{\Delta M^2}}{\overline{M}^2} \tag{10}$$

where $\overline{M} = \frac{\sum_n c_n \sum_i f_{i,n} M_{i,n}}{\sum_n c_n}$, $\overline{\Delta M} = \frac{\sum_n c_n \sum_i f_{i,n} (M_{i,n} - \overline{M_n})^2}{\sum_n c_n}$, $\overline{M_n} = \sum_i f_{i,n} M_{i,n}$, c_n is the stoichiometry of the n-th component and $f_{i,n}$ is the fraction of the i-th element that is presented in the n-th component. Using this formulation, the effect of the material composition can be inferred from the lattice thermal conductivity.

Effective medium approximation, on the other hand, presents a more simplified version of the formula described above. The model incorporates an interface resistance, called Kapitza resistance (R_κ), in series with the inter grain resistance [167]. This model is further developed to consider the shapes, orientations, volume fractions, and thermal conductivities of the phases [160]. For instance, the thermal conductivity of a two-phase material with spherical inclusions is expressed by:

$$\kappa^* = \kappa_m \frac{\kappa_p(1 + 2\alpha) + 2\kappa_m + 2f\left[\kappa_p(1 - \alpha) - \kappa_r\right]}{\kappa_p(1 + 2\alpha) + 2\kappa_m - f\left[\kappa_p(1 - \alpha) - \kappa_r)\right]} \tag{11}$$

where κ_m is the thermal conductivity of the matrix, κ_p is the thermal conductivity of the secondary phase, and f is the volume fraction of the secondary phase. The non-dimensional parameter, α, is the ratio of the Kapitza length, L_κ, and the second phase radius, a:

$$\alpha = \frac{L_\kappa}{a} = \frac{\kappa_m R_\kappa}{a} \tag{12}$$

An even more simple model than that which has been used to describe the scattering in multiphase materials is impedance mismatch [152]. The specific acoustic impedance of a material is the analogue of the electrical impedance for electrical circuits. In this case, the acoustic impedance measures the opposition of a system when acoustic pressure is applied to it and its calculated as:

$$Z = \rho v \tag{13}$$

where ρ is the volumetric density of the medium and ν_S is the speed of the sound in the medium. At the interface of two materials, the reflection (r) and transmission (t) energy coefficients are [168]:

$$r = \left[\frac{Z_2 - Z_1}{Z_2 + Z_1}\right]^2, \quad t = \frac{4Z_1 Z_2}{(Z_1 + Z_2)^2} \tag{14}$$

where Z_1 and Z_2 are the acoustic impedance of the two materials. Figure 6 illustrates phonon transmission and reflection between two dissimilar materials.

Experimentally, impedance mismatch between phases has been shown to reduce the thermal conductivity of the bulk material. The impedance mismatch between the PbTe and PbS rich phases in $(Pb_{0.95}Sn_{0.05}Te)_{1-x}(PbS)_x$ samples led to an inhibition of the heat flow, with the lattice thermal conductivity reaching 0.4 W·m^{-1}·K^{-1} for the sample with 8% PbS, an 80% reduction in the reported values for the bulk material [169].

$Z_1 \neq Z_2$

$$t = \frac{4Z_1 Z_2}{(Z_1 + Z_2)^2}$$

$$r = \left[\frac{Z_2 - Z_1}{Z_2 + Z_1} \right]^2$$
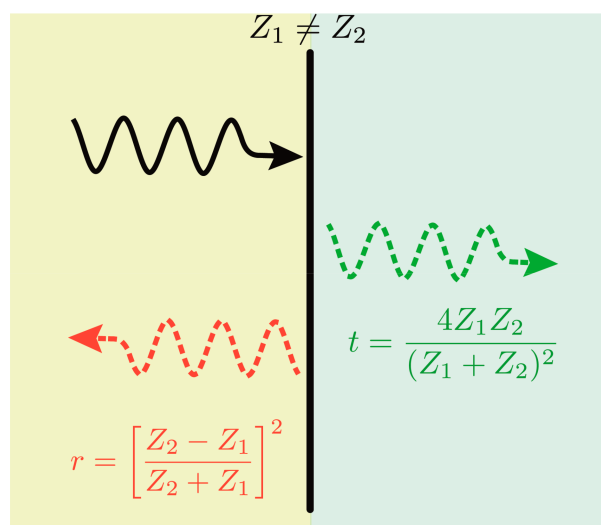
Figure 6. Phonon transmission and reflection due to impedance mismatch.

In general, phonon scattering has proven to be an effective strategy to reduce the lattice thermal conductivity in multiphase lead telluride-based materials [170–173] and bismuth telluride-based [174–176] materials. For instance, nano-engineered multiphase PbTe—x% InSb compounds showed an exceptionally low minimum lattice thermal conductivity of ~0.3 W·m^{-1}·K^{-1} at ~770 K for 4% InSb and consequently a zT value of ~1.83 at 770 K [177]. Even higher zT values of ~2 were observed for $Pb_{(1-x)}Na_x Te_{0.65}S_{0.25}Se_{0.1}$ compounds [30,31], where the combined effects of phonon scattering at nanoprecipitates and the increase in the power factor due to heterogeneous distribution of dopants between phases were recognised to be responsible for the high TE efficiency. Nano and micro-sized precipitates in $Pb_{1-x}Ga_x Te$ (x = 0.01, 0.02, 0.03, and 0.04) compounds have shown a reduction in the lattice thermal conductivity, reaching 1.6 W·m^{-1}·K^{-1}. A larger fraction of a secondary phase with high thermal conductivity can increase the total thermal conductivity, reported for PbTe-Ge$_x$ [178]. Five per cent of GeTe reduced the lattice thermal conductivity to 1.1 W·m^{-1}·K^{-1}, while a sample with x = 0.2 showed a lattice thermal conductivity similar to the pristine sample.

Adding a secondary phase of TiO_2 to a Bi_2Se_3 host increased the Seebeck coefficient by energy filtering and simultaneously reduced the lattice thermal conductivity by 45% [101]. The lattice thermal conductivity of multiphase half-Heusler $(Hf_{0.6}Zr_{0.4})NiSn_{0.99}Sb_{0.01}$ material was reduced from ~4.5 W·m^{-1}·K^{-1} for the pristine sample to ~2.9 W·m^{-1}·K^{-1} for the sample with 20wt.% of tungsten at 300 K [112]; the combined effects of phonon scattering and energy filtering due to the presence of metallic tungsten improved the zT by 55%.

The lattice thermal conductivity values of several single-phase chalcogenides are compared with their multiphase counterparts in Figure 7. The data for single-phase materials were manually extracted from the Materials Research Laboratory Energy Materials Datamining website [179,180]. This dataset contains information of 573 thermoelectric materials from various combinations of host materials and dopants along with several thermoelectric properties measured experimentally at 300 K, 400 K, and 700 K. Here, we have selected the lattice thermal conductivity of chalcogenides, measured at 300 K. Where the lattice thermal conductivity was not available, its value was evaluated using the Wiedemann–Franz law and the Sommerfeld limit for the Lorenz number [181]. Both the bar and boxplot show that the multiphase materials consistently present lower values of the lattice thermal conductivity. In particular, the boxplot shows that the multiphase materials have, on average, lower values of lattice thermal conductivity.
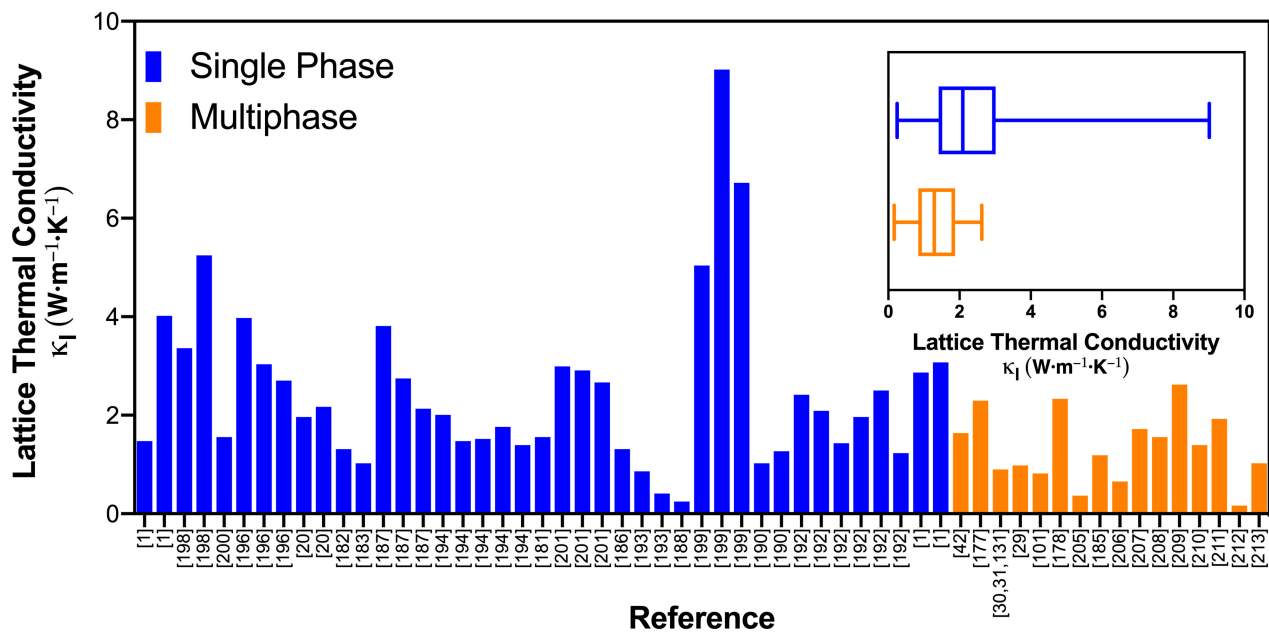
Figure 7. The lattice thermal conductivity of multiphase thermoelectric materials compared with single-phase counterparts; data extracted from [1,20,29–31,42,101,131,177,178,182–213]. The inset shows a boxplot of the same data.

5. Models to Estimate the Transport Properties

In general, multiphase materials can increase phonon scattering, increase the Seebeck coefficient due to energy filtering, and increase electrical conductivity due to modulation doping. These micro and nano effects clearly influence the material on a macroscale. It is, however, of interest to have simplified expressions to predict the behaviour of these materials from the composition and electronic band engineering perspectives. Regarding the thermal conductivity, the effective medium theory allows us to approximate the effective Seebeck coefficient and the electrical conductivity of multiphase materials [214]. There are two main equations to evaluate these properties. The most common equation is the one derived from the usual effective mean theory [215]:

$$\sum_i v_i \frac{\zeta_i - \zeta}{\zeta_i + 2\zeta} = 0 \qquad (15)$$

where v_i and ζ_i are the volume fraction and property of phase i, respectively, and ζ is the effective material property. The electrical conductivity can be calculated by setting $\zeta = \sigma$, and the Seebeck coefficient can be calculated by setting $\zeta = S/\sigma$ [216]. The second equation is based on the generalised effective mean theory:

$$\sum_i v_i \frac{\zeta_i^{\frac{1}{t}} - \zeta^{\frac{1}{t}}}{\zeta_i^{\frac{1}{t}} + A \cdot \zeta^{\frac{1}{t}}} = 0 \qquad (16)$$

where t is a measure of the grain structure and morphology, and $A = (1 - p_c)/p_c$, where p_c is the percolation threshold. Both parameters can be determined by fitting experimental data, and p_c is estimated from the lattice type and dimensions of the network [217]. The Seebeck coefficient and the conductivity are estimated similar to the previous equation [218].

Recently, models based on electrical networks have been introduced to estimate the electronic properties [214,219,220] and finite element analysis [221]. These latter models divide the material into pixels (for a 2D analysis) or voxels (for a 3D analysis) grids, where each node corresponds to a fraction of the total volume. Each voxel/pixel is required to be larger than the mean free paths of the carriers and phonons so that the transport is diffusive.

Each node is connected to its neighbours by a resistance that is an electric resistance (to calculate the electrical conductivity) and a thermal resistance (to calculate the thermal conductivity) in series with an interface resistance if needed. Following the construction of grids, a nodal analysis will be conducted [222] to determine the temperature and voltage profile of the grids. The Seebeck coefficient is estimated by assigning each node in the electric grid to a local voltage source in series, representing the local Seebeck voltage. By using a Norton equivalent of the voltage source [223], the usual nodal formulation can be applied, and the bulk Seebeck coefficient will be estimated. The general expression is presented as [220]:

$$0 = \sum_{k \neq l} V_{kl} G_{kl} + \sum_{k \neq l} I_{kl} \tag{17}$$

where $V_{k,l}$ is the voltage (or temperature) difference between nodes k and l, $I_{k,l}$ is the current flowing between nodes k and l, and $G_{k,l}$ is the conductivity between nodes k and l. The conductivity will be determined by the local thermoelectric properties of the voxels or pixels:

$$\sigma_{kl}^{-1} = \sigma_k^{-1} + \sigma_l^{-1}, \ \kappa_{kl}^{-1} = \kappa_k^{-1} + \kappa_l^{-1} \tag{18}$$

where σ_k, σ_l is the electrical conductivity of nodes k and l, respectively, and κ_k, κ_l is the thermal resistivity of nodes k and l.

The main advantage of this approach is that this linear system of equations can easily be solved by electric circuit solvers, and the results can be directly interpreted by engineers. However, the quantum effects are not approximated by an effective medium theory in this model, and therefore, it provides similar accuracy to the more simple models described earlier [219]. Overall, from a design perspective, these equations suggest that the incorporation of highly conductive phases (both thermally and electrically) results in an overall increase in the conductivity of materials. This effect has been experimentally proven in several materials. Graphene, a zero-bandgap material [224], has been successfully used to create thermoelectric materials with high conductivity [225–227], the electrical conductivity of $CoSb_3$ reached 1.2×10^6 S/m, four times larger than the pristine sample at 300 K [226]. Copper telluride in $Bi_{0.5}Sb_{1.5}Te_3$ [228] and a composite of ZnSb matrix with minority phases of Zn_4Sb_3, Zn_3P_2, and Cu_5Zn_8 [229] have shown higher electrical conductivity. It should be noted that the values of electronic transport properties are greatly dependent on the fabrication methods [230], quality of the raw materials, and oxidisation of the material [231–233].

High-temperature, oxide-based thermoelectric materials have also been shown to benefit from the presence of secondary phases. A multiphase compound of $Ca_3Co_4O_9$, matrimid polymer + Ag, and carbon black [40] showed a reduction in the electrical conductivity compared to the porous $Ca_3Co_4O_9$, while the highly conductive phase of Ag reduced a significant deterioration of conductivity.

6. Magnetic Effects

The effects of magnetism on the performance of thermoelectric materials have been investigated for some time, but with less detailed analysis. The idea of spin-wave scattering and magnon drag was proposed in the middle of the last century, where magnon scattering was shown to contribute to an increase in the Seebeck coefficient [234]. Magnons are bosonic quasiparticles, the quanta associated with spin waves [235]. When a magnetic material is subjected to a temperature gradient, the hotter side contains a higher density of magnons that will diffuse towards the cooler side; this magnon flux "drags" the free charge carriers due to the electron–magnon collisions and gives rise to a second contribution to the Seebeck coefficient, called the magnon thermopower [236]. A hydrodynamical, Galilean based expression for the magnon thermopower is [237]

$$S_{md} = \frac{2}{3} \cdot \frac{C_m}{n_e e} \cdot \frac{1}{1 + \frac{\tau_{em}}{\tau_m}} \tag{19}$$

where C_m is the magnon specific heat capacity per unit volume, τ_m and τ_{em} are, respectively, the transport mean-free time for the electron and magnon–electron collision, e is carrier charge, and n_e is the charge carrier density.

When dealing with magnetism in semiconductors, three main strategies have been proposed to improve the thermoelectric efficiency: (1) optimise thermoelectric properties of magnetic materials using strategies known for non-magnetic materials [43–45,238,239]; (2) introduce a magnetic dopant in a non-magnetic material [46–48,240–243]; (3) introduce a magnetic secondary phase in a non-magnetic material [49,50].

6.1. Magnetic Semiconductors

Examples of magnetic semiconductors are $FeSb_2$ [244,245], MnTe [246–248], $Cr_2Ge_2Te_6$ [249], MgAgSb [250], MnSe [251], and FeSe [252]. Experimental results have shown their potential as thermoelectric materials; for instance, a massive Seebeck coefficient of ~27 mV/K has been reported for $FeSb_2$ (albeit at a low temperature of ~12 K) [253]. It is not easy, however, to establish a causal relationship between magnetism and the Seebeck coefficient. A common method is to check whether a heavily doped sample with a high carrier concentration shows a large value of the Seebeck coefficient [254], because this indicates a possible effect of electron–magnon scattering, which increases the Seebeck coefficient. Fitting mathematical models to the experimental data has also been proposed as a method to identify the magnetic thermopower [255]. Clearly, measuring the transport properties as a function of the magnetic field is the best method to determine the magnetic thermopower [236,256,257].

A spin-dependent Seebeck coefficient can occur in magnetic semiconductors [258]; since the Seebeck coefficients for the two spin channels of spin-up ($S^\uparrow$) and spin-down ($S^\downarrow$) are not equal, a spin current proportional to the difference between $S^\uparrow$ and $S^\downarrow$ flows through the magnetic material even in the absence of a charge current [259]. The literature refers to spintronics as the field of study that investigates devices that exploit the properties of electrons spins. In thermoelectricity, this is known as spin caloritronic [260]. This new field of research has attracted the interest of the thermoelectric research community [261–263].

6.2. Magnetic Dopants in Non-Magnetic Semiconductors

Doping non-magnetic thermoelectric materials with magnetic elements has improved the power factor. Magnetic doping of $CuGaTe_2$ with manganese ions (Mn^{2+}) increased the effective mass of the carriers due to the interaction of the magnetic ions and the charge carriers and, consequently, increased the Seebeck coefficient [264]. This effect has also been reported for a Chromium doped Bi_2Te_3 [265]. The negative side effect of magnetic ion dopants is the decrease in the charge carrier mobility that results in a reduction in the electrical conductivity. Overall, the power factor is shown to be increased [266–268].

6.3. Secondary Magnetic Phases

The natural extension of using magnetic elements is to include magnetic phases to enhance the performance of thermoelectric materials [264,269,270]. The magnetic particles of $BaFe_{12}O_{19}$ in $Ba_{0.3}In_{0.3}Co_4Sb_{12}$ formed a magnetic composite; $BaFe_{12}O_{19}$ nanoparticles trap electrons in the ferromagnetic phase due to the spiral motion of the electrons generated by non-uniform spherical magnetic fields. This effectively suppresses the deterioration of thermoelectric efficiency in the intrinsic excitation region [271]. In the paramagnetic phase (at temperatures above the Curie temperature), though, the nanoparticles release the trapped electrons to increase the carrier concentration in the intrinsic excitation. This effect enhances the overall performance of the thermoelectric material.

Coherent magnetic full-Heusler nanoparticles ($Ti(Ni_{4/3}Fe_{2/3})Sn$) in a half-Heusler matrix ($Ti_{0.25}Zr_{0.25}Hf_{0.5}NiSn_{0.975}Sb_{0.025}$) showed significant enhancements of both carrier mobility and the Seebeck coefficient [272]. The magnetic nanoparticles interact with the spin of itinerant carriers, leading to charge localisation (which consequently leads to a decrease in the charge density) and the formation of overlapping bound magnetic polarons (that leads to an increase in mobility).

Interestingly, some magnetic phenomena only occur when the particles are smaller than a certain size [273]. Nanoparticles provide a good platform to take advantage of these magnetic phenomena for the purpose of optimising the thermoelectric performance of materials. If the size of a ferromagnetic nanoparticle is small enough to have only several magnetic domains, it can be magnetised similar to a paramagnet under an external magnetic field, except with a much greater magnetisation. This mechanism is known as superparamagnetism (magnetisation of the nanoparticles can randomly flip direction under the influence of temperature, and they can be magnetised similar to a paramagnet under an external magnetic field [274]). Experimentally, soft magnet transition metals (Fe, Co, or Ni) nanoparticles were embedded in a $Ba_{0.3}In_{0.3}Co_4Sb_{12}$ matrix [275]. The superparamagnetism fluctuations of the nanoparticles gave rise to multiple scattering of electrons and enhanced phonon scattering. These effects increased the overall thermoelectric efficiency of the material.

In general, secondary magnetic phases introduce a new degree of freedom to enhance thermoelectric materials. The effects of magnetism in semiconductors are not fully understood yet, and general expressions for the contribution of the magnon-drag on the Seebeck coefficient are unavailable yet. The need for more experimental and theoretical investigation presents an opportunity for thermoelectricity.

Table 3 summarises the sample composition and fabrication techniques of recent studies that reported magnetic effects in thermoelectric materials.

Table 3. Sample composition, fabrication technique, and corresponding references which studied magnetic effects in thermoelectric materials.

System	Fabrication Method	Type	Ref.
$CuGa_{1-x}Mn_xTe_2$ (x = 0, 0.01, 0.02, and 0.03)	Casting + hand milling + sintering	Magnetic dopant	[264]
$Bi_{2-x}Cr_xTe_3$ (x = 0, 0.01, 0.02, 0.05, and 0.10)	Casting + hand milling + sintering	Magnetic dopant	[265]
$Fe_{3-x}Ti_xSn$ (x = 0, 0.25, 0.5, 0.75)	Casting	Magnetic material	[239]
$Sn_{1.03-x}Mn_xTe$ (x = 0, 0.05, 0.07, and 0.1)	Casting + cold pelletising	Magnetic dopant	[266]
$Ba_{0.3}In_{0.3}Co_4Sb_{12}$ +x $BaFe_{12}O_{19}$) (x = 0.15%, 0.25%, 0.35%, and 0.45%)	Ball milling + sintering	Magnetic phase	[271]
$Ti_{0.25}Zr_{0.25}Hf_{0.5}(Ni,Fe_x)Sn_{0.975}Sb_{0.025}$ (x = 0, 0.05, 0.01, 0.15)	Casting + hand milling + sintering	Magnetic phase	[272]
$Mn_{1-x}Na_xSe$ ($0 \leq x \leq 0.03$)	Ball milling + annealing + hot pressing	Magnetic material	[251]
$FeSb_2$	Hand milling + annealing + hot pressing	Magnetic material	[244]

Figure 8 compares the maximum zT values reported for several single chalcogenides with their multiphase counterparts. The data for single-phase materials were manually extracted from the Materials Research Laboratory Energy Materials Datamining website [179,180]. Both the bar and violin plot show that the multiphase materials consistently present larger values of zT. In particular, the violin plot shows that many single-phase materials have low zT, while the zT for multiphase materials is distributed towards larger values.
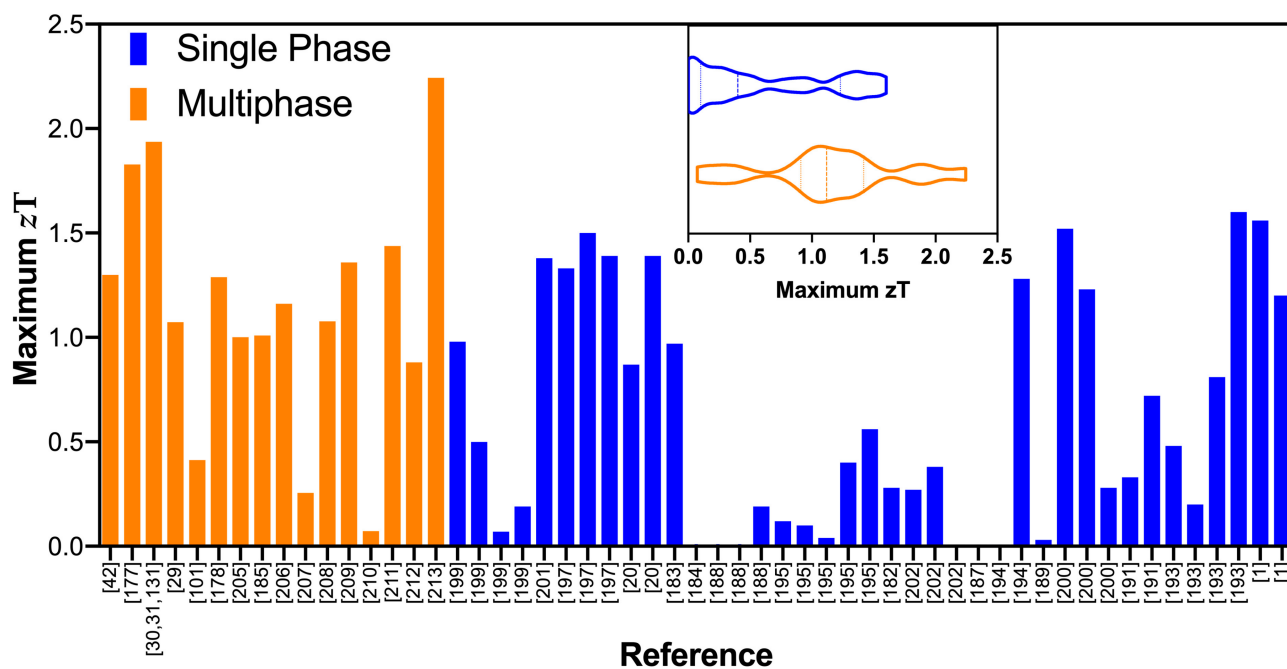
Figure 8. *z*T values of multiphase thermoelectric materials compared with single-phase counterparts; data extracted from [1,20,29–31,42,101,131,177,178,182–213]. The inset shows the truncated violin plot of the same data, where the dashed line represents the median and dotted lines represent the quartiles.

7. Summary and Outlook

Here, we have reviewed the principal mechanisms and strategies employed to enhance the thermoelectric efficiency of multiphase thermoelectric materials. The interfaces between phases in a material can be utilised to construct potential barriers in the electronic band structure and perform an energy filtering on the charge carriers, where the low energy charge carriers will be filtered/scattered. This can increase the average energy at which the electronic conduction occurs and consequently increase the Seebeck coefficient. The effect of the barrier height can be estimated from the relaxation time approximation from the Boltzmann equation. For a metallic secondary phase, the potential barrier height can be estimated from the work function of the metal and electron affinity of the semiconductor following Schottky's rule. For heterojunctions (two different semiconductors), the potential barrier is proportional to the difference of the electron affinities between the two materials and can be estimated from Anderson's rule. Experimental results have shown that the energy-filtering effect can increase the Seebeck coefficient while decreasing electrical conductivity. The overall result, however, is an increase in the power factor.

Modulation doping is a well-known technique for enhancing the conductivity of semiconductor devices. In this paper, we briefly reviewed the mechanism by which modulation doping is used in multiphase thermoelectric materials.

An increase in phonon scattering due to the presence of secondary phases improves the thermoelectric efficiency of these materials. Secondary phases decrease the relaxation time of the phonons. Traditional models can be employed to verify the effect of a secondary phase on the thermal conductivity of materials. The Klemens model has been used to theoretically explain the reduction in thermal conductivity. The effective medium approximation has been promising in describing the phonon scattering mechanisms of materials with simple structures, such as spherical particles. In an even more simplistic view, for some materials, the transmission and reflection coefficients determined based on the acoustic impedance of the primary and secondary phases can be readily used to evaluate the effect of multiple phases on the reduction of thermal conductivity. Experimentally, a large increase in the *z*T has been reported with the use of secondary phases.

Mathematical models based on effective medium theory and networks can also estimate the Seebeck coefficient and electrical conductivity of multiphase materials. These models can be used as a tool to evaluate and tune the properties of thermoelectric materials.

The incorporation of magnetic doping elements and secondary phases in thermoelectric materials has introduced new possibilities to enhance their efficiency. The scattering of electrons due to interactions between charge carriers and magnons can contribute to an increase in the Seebeck coefficient. A magnon flux generated from a temperature gradient "drags" the free carriers and contributes positively to the Seebeck coefficient—this effect is called the magnon thermopower. Experimentally, this has proven to be a promising strategy to enhance the thermoelectric properties of several materials.

Overall, multiphase materials have been shown to be instrumental in achieving high thermoelectric efficiency. Multiple phases allow for more degrees of freedom in the materials design as each phase can be finely tuned to improve selected properties of the multiphase material.

References

1. Biswas, K.; He, J.; Blum, I.D.; Wu, C.I.; Hogan, T.P.; Seidman, D.N.; Dravid, V.P.; Kanatzidis, M.G. High-Performance Bulk Thermoelectrics with All-Scale Hierarchical Architectures. *Nature* **2012**, *489*, 414–418. [CrossRef] [PubMed]
2. Vining, C.B. An Inconvenient Truth about Thermoelectrics. *Nat. Mater.* **2009**, *8*, 83–85. [CrossRef]
3. Tritt, T.M.; Boettner, H.; Chen, L. Thermoelectrics: Direct Solar Thermal Energy Conversion. *MRS Bull.* **2008**, *33*, 366–368. [CrossRef]
4. Cutler, M.; Mott, N.F. Observation of Anderson Localization in an Electron Gas. *Phys. Rev.* **1969**, *181*, 1336–1340. [CrossRef]
5. Siemens, M.E.; Li, Q.; Yang, R.; Nelson, K.A.; Anderson, E.H.; Murnane, M.M.; Kapteyn, H.C. Quasi-Ballistic Thermal Transport from Nanoscale Interfaces Observed Using Ultrafast Coherent Soft X-Ray Beams. *Nat. Mater.* **2010**, *9*, 26–30. [CrossRef]
6. Delaire, O.; Ma, J.; Marty, K.; May, A.F.; McGuire, M.A.; Du, M.H.; Singh, D.J.; Podlesnyak, A.; Ehlers, G.; Lumsden, M.D.; et al. Giant Anharmonic Phonon Scattering in PbTe. *Nat. Mater.* **2011**, *10*, 614–619. [CrossRef] [PubMed]
7. Hu, Y.; Zeng, L.; Minnich, A.J.; Dresselhaus, M.S.; Chen, G. Spectral Mapping of Thermal Conductivity through Nanoscale Ballistic Transport. *Nat. Nanotechnol.* **2015**, *10*, 701–706. [CrossRef]
8. Hu, L.; Zhang, Y.; Wu, H.; Li, J.; Li, Y.; McKenna, M.; He, J.; Liu, F.; Pennycook, S.J.; Zeng, X. Entropy Engineering of SnTe: Multi-Principal-Element Alloying Leading to Ultralow Lattice Thermal Conductivity and State-of-the-Art Thermoelectric Performance. *Adv. Energy Mater.* **2018**, *8*, 1802116. [CrossRef]
9. Fan, Z.; Wang, H.; Wu, Y.; Liu, X.J.; Lu, Z.P. Thermoelectric High-Entropy Alloys with Low Lattice Thermal Conductivity. *RSC Adv.* **2016**, *6*, 52164–52170. [CrossRef]
10. Wei, P.C.; Liao, C.N.; Wu, H.J.; Yang, D.; He, J.; Biesold-McGee, G.V.; Liang, S.; Yen, W.T.; Tang, X.; Yeh, J.W.; et al. Thermodynamic Routes to Ultralow Thermal Conductivity and High Thermoelectric Performance. *Adv. Mater.* **2020**, *32*, e1906457. [CrossRef]
11. Joshi, G.; Lee, H.; Lan, Y.; Wang, X.; Zhu, G.; Wang, D.; Gould, R.W.; Cuff, D.C.; Tang, M.Y.; Dresselhaus, M.S.; et al. Enhanced Thermoelectric Figure-of-Merit in Nanostructured p-Type Silicon Germanium Bulk Alloys. *Nano Lett.* **2008**, *8*, 4670–4674. [CrossRef]
12. Wang, X.W.; Lee, H.; Lan, Y.C.; Zhu, G.H.; Joshi, G.; Wang, D.Z.; Yang, J.; Muto, A.J.; Tang, M.Y.; Klatsky, J.; et al. Enhanced Thermoelectric Figure of Merit in Nanostructured N-Type Silicon Germanium Bulk Alloy. *Appl. Phys. Lett.* **2008**, *93*, 193121. [CrossRef]
13. Lan, Y.C.; Minnich, A.J.; Chen, G.; Ren, Z.F. Enhancement of Thermoelectric Figure-of-Merit by a Bulk Nanostructuring Approach. *Adv. Funct. Mater.* **2010**, *20*, 357–376. [CrossRef]

14. Ren, Z.; Poudel, B.E.D.; Chen, G.; Lan, Y.; Wang, D.; Hao, Q.; Dresselhaus, M.; Ma, Y.I.; Yan, X.; Chen, X.; et al. Methods for High Figure-of-Merit in Nanostructured Thermoelectric Materials. U.S. Patent 8865995B2, 21 October 2014.

15. Yu, B.; Zebarjadi, M.; Wang, H.; Lukas, K.; Wang, H.; Wang, D.; Opeil, C.; Dresselhaus, M.; Chen, G.; Ren, Z. Enhancement of Thermoelectric Properties by Modulation-Doping in Silicon Germanium Alloy Nanocomposites. *Nano Lett.* **2012**, *12*, 2077–2082. [CrossRef]

16. Wang, H.; Cao, X.; Takagiwa, Y.; Snyder, G.J. Higher Mobility in Bulk Semiconductors by Separating the Dopants from the Charge-Conducting Band—A Case Study of Thermoelectric PbSe. *Mater. Horiz.* **2015**, *2*, 323–329. [CrossRef]

17. Thesberg, M.; Pourfath, M.; Kosina, H.; Neophytou, N. The Influence of Non-Idealities on the Thermoelectric Power Factor of Nanostructured Superlattices. *J. Appl. Phys.* **2015**, *118*, 224301. [CrossRef]

18. Rhyee, J.S.; Lee, K.H.; Lee, S.M.; Cho, E.; Kim, S.I.; Lee, E.; Kwon, Y.S.; Shim, J.H.; Kotliar, G. Peierls Distortion as a Route to High Thermoelectric Performance in In(4)Se(3-Delta) Crystals. *Nature* **2009**, *459*, 965–968. [CrossRef] [PubMed]

19. Zhou, J.; Yang, R.; Chen, G.; Dresselhaus, M.S. Optimal Bandwidth for High Efficiency Thermoelectrics. *Phys. Rev. Lett.* **2011**, *107*, 226601. [CrossRef] [PubMed]

20. Heremans, J.P.; Jovovic, V.; Toberer, E.S.; Saramat, A.; Kurosaki, K.; Charoenphakdee, A.; Yamanaka, S.; Snyder, G.J. Enhancement of Thermoelectric Efficiency in PbTe by Distortion of the Electronic Density of States. *Science* **2008**, *321*, 554–557. [CrossRef]

21. Mao, J.; Liu, Z.; Ren, Z. Size Effect in Thermoelectric Materials. *npj Quant. Mater.* **2016**, *1*, 16028. [CrossRef]

22. Zeng, G.; Bowers, J.E.; Zide, J.M.O.; Gossard, A.C.; Kim, W.; Singer, S.; Majumdar, A.; Singh, R.; Bian, Z.; Zhang, Y.; et al. ErAs:InGaAs/InGaAlAs Superlattice Thin-Film Power Generator Array. *Appl. Phys. Lett.* **2006**, *88*, 113502. [CrossRef]

23. Zebarjadi, M.; Joshi, G.; Zhu, G.; Yu, B.; Minnich, A.; Lan, Y.; Wang, X.; Dresselhaus, M.; Ren, Z.; Chen, G. Power Factor Enhancement by Modulation Doping in Bulk Nanocomposites. *Nano Lett.* **2011**, *11*, 2225–2230. [CrossRef] [PubMed]

24. Hou, Q.R.; Gu, B.F.; Chen, Y.B.; He, Y.J.; Sun, J.L. Enhancement of the Thermoelectric Power Factor of MnSi1.7 Film by Modulation Doping of Al and Cu. *Appl. Phys. A Mater.* **2014**, *114*, 943–949. [CrossRef]

25. Gu, Y.; Ai, W.; Zhao, Y.; Pan, L.; Lu, C.; Zong, P.; Hu, X.; Xu, Z.; Wang, Y. Remarkable Thermoelectric Property Enhancement in Cu_2SnS_3–$CuCo_2S_4$ Nanocomposites via 3D Modulation Doping. *J. Mater. Chem. A* **2021**, *9*, 16928–16935. [CrossRef]

26. Wu, L.H.; Li, X.; Wang, S.Y.; Zhang, T.S.; Yang, J.; Zhang, W.Q.; Chen, L.D.; Yang, J.H. Resonant Level-Induced High Thermoelectric Response in Indium-Doped GeTe. *NPG Asia Mater.* **2017**, *9*, e343. [CrossRef]

27. Zhang, Q.Y.; Wang, H.; Liu, W.S.; Wang, H.Z.; Yu, B.; Zhang, Q.; Tian, Z.T.; Ni, G.; Lee, S.; Esfarjani, K.; et al. Enhancement of Thermoelectric Figure-of-Merit by Resonant States of Aluminium Doping in Lead Selenide. *Energy Environ. Sci.* **2012**, *5*, 5246–5251. [CrossRef]

28. Kim, R.; Lundstrom, M.S. Computational Study of Energy Filtering Effects in One-Dimensional Composite Nano-Structures. *J. Appl. Phys.* **2012**, *111*, 024508. [CrossRef]

29. Yamini, A.; Li, T.; Mitchell, D.R.G.; Cairney, J.M. Elemental Distributions within Multiphase Quaternary Pb Chalcogenide Thermoelectric Materials Determined through Three-Dimensional Atom Probe Tomography. *Nano Energy* **2016**, *26*, 157–163. [CrossRef]

30. Aminorroaya Yamini, S.; Mitchell, D.R.; Avdeev, M. In Situ Characterisation of Nanostructured Multiphase Thermoelectric Materials at Elevated Temperatures. *Phys. Chem. Chem. Phys.* **2016**, *18*, 32814–32819. [CrossRef]

31. Byrnes, J.; Mitchell, D.R.G.; Yamini, S.A. Thermoelectric Performance of Thermally Aged Nanostructured Bulk Materials-a Case Study of Lead Chalcogenides. *Mater. Today Phys.* **2020**, *13*, 100190. [CrossRef]

32. Gao, Y.-H.; Chen, H.; Liu, N.; Zhang, R.-Z. Criteria for Power Factor Improvement in Thermoelectric Composite. *Results Phys.* **2018**, *11*, 915–919. [CrossRef]

33. Hu, Q.; Qiu, W.; Chen, L.; Chen, J.; Yang, L.; Tang, J. Realize High Thermoelectric Properties in N-Type $Bi_2Te_{2.7}Se_{0.3}/Y_2O_3$ Nanocomposites by Constructing Heterointerfaces. *ACS Appl. Mater. Interfaces* **2021**, *13*, 38526–38533. [CrossRef] [PubMed]

34. Pham, A.T.T.; Vo, P.T.N.; Ta, H.K.T.; Lai, H.T.; Tran, V.C.; Doan, T.L.H.; Duong, A.T.; Lee, C.T.; Nair, P.K.; Zulueta, Y.A.; et al. Improved Thermoelectric Power Factor Achieved by Energy Filtering in ZnO: Mg/ZnO Hetero-Structures. *Thin Solid Films* **2021**, *721*, 138537. [CrossRef]

35. Park, W.; Hwang, H.; Kim, S.; Park, S.; Jang, K.-S. Optimized Thermoelectric Performance of Carbon Nanoparticle–Carbon Nanotube Heterostructures by Tuning Interface Barrier Energy. *ACS Appl. Mater. Interfaces* **2021**, *13*, 7208–7215. [CrossRef] [PubMed]

36. Lee, M.H.; Yun, J.H.; Kim, G.; Lee, J.E.; Park, S.-D.; Reith, H.; Schierning, G.; Nielsch, K.; Ko, W.; Li, A.-P.; et al. Synergetic Enhancement of Thermoelectric Performance by Selective Charge Anderson Localization–Delocalization Transition in n-Type Bi-Doped $PbTe/Ag_2Te$ Nanocomposite. *ACS Nano* **2019**, *13*, 3806–3815. [CrossRef]

37. Wang, C.; Lin, S.; Chen, H.; Zhao, Y.; Zhao, L.; Wang, H.; Huo, D.; Chen, X. Thermoelectric Performance of $Si_{80}Ge_{20-x}Sb_x$ Based Multiphase Alloys with Inhomogeneous Dopant Distribution. *Energy Convers. Manag.* **2015**, *94*, 331–336. [CrossRef]

38. Wu, D.; Pei, Y.; Wang, Z.; Wu, H.; Huang, L.; Zhao, L.-D.; He, J. Significantly Enhanced Thermoelectric Performance in N-Type Heterogeneous BiAgSeS Composites. *Adv. Funct. Mater.* **2014**, *24*, 7763–7771. [CrossRef]

39. Ahmad, K.; Wan, C.; Al-Eshaikh, M.A.; Kadachi, A.N. Enhanced Thermoelectric Performance of Bi_2Te_3 Based Graphene Nanocomposites. *Appl. Surf. Sci.* **2019**, *474*, 2–8. [CrossRef]

40. Wolf, M.; Menekse, K.; Mundstock, A.; Hinterding, R.; Nietschke, F.; Oeckler, O.; Feldhoff, A. Low Thermal Conductivity in Thermoelectric Oxide-Based Multiphase Composites. *J. Electron. Mater.* **2019**, *48*, 7551–7561. [CrossRef]

41. Manimozhi, T.; Kavirajan, S.; Harish, S.; Archana, J.; Kamala Bharathi, K.; Senthil Kumar, E.; Navaneethan, M. Anharmonicity and Low-Thermal Conductivity in the Multi-Phase Composition of $Cu_3Bi_{0.75}Sb_{0.25}S_3$. *Mater. Lett.* **2021**, *304*, 130399. [CrossRef]

42. Wang, Z.; Wang, G.; Wang, R.; Zhou, X.; Chen, Z.; Yin, C.; Tang, M.; Hu, Q.; Tang, J.; Ang, R. Ga-Doping-Induced Carrier Tuning and Multiphase Engineering in n-Type PbTe with Enhanced Thermoelectric Performance. *ACS Appl. Mater. Interfaces* **2018**, *10*, 22401–22407. [CrossRef]

43. Sun, P.; Oeschler, N.; Johnsen, S.; Iversen, B.B.; Steglich, F. Thermoelectric Properties of the Narrow-Gap Semiconductors $FeSb_2$ and $RuSb_2$: A Comparative Study. *J. Phys. Conf. Ser.* **2009**, *150*, 012049. [CrossRef]

44. Sun, Y.; Canulescu, S.; Sun, P.J.; Steglich, F.; Pryds, N.; Schou, J.; Iversen, B.B. Growth and Thermoelectric Properties of $FeSb_2$ Films Produced by Pulsed Laser Deposition. *Appl. Phys. A Mater.* **2011**, *104*, 883–887. [CrossRef]

45. Tsujii, N.; Mori, T.; Isoda, Y. Phase Stability and Thermoelectric Properties of $CuFeS_2$-Based Magnetic Semiconductor. *J. Electron. Mater.* **2014**, *43*, 2371–2375. [CrossRef]

46. Motohashi, T.; Naujalis, E.; Ueda, R.; Isawa, K.; Karppinen, M.; Yamauchi, H. Simultaneously Enhanced Thermoelectric Power and Reduced Resistivity of $NaxCo_2O_4$ by Controlling Na Nonstoichiometry. *Appl. Phys. Lett.* **2001**, *79*, 1480–1482. [CrossRef]

47. Wen, Q.; Chang, C.; Pan, L.; Li, X.T.; Yang, T.; Guo, H.H.; Wang, Z.H.; Zhang, J.; Xu, F.; Zhang, Z.D.; et al. Enhanced Thermoelectric Performance of BiCuSeO by Increasing Seebeck Coefficient through Magnetic Ion Incorporation. *J. Mater. Chem. A* **2017**, *5*, 13392–13399. [CrossRef]

48. Xiao, C.; Li, K.; Zhang, J.J.; Tong, W.; Liu, Y.W.; Li, Z.; Huang, P.C.; Pan, B.C.; Su, H.B.; Xie, Y. Magnetic Ions in Wide Band Gap Semiconductor Nanocrystals for Optimized Thermoelectric Properties. *Mater. Horiz.* **2014**, *1*, 81–86. [CrossRef]

49. Liu, K.G.; Li, J. Thermoelectric Properties of Bulk $FeSb_2$ and the Composite of $FeSb_2$ and $CoSb_3$ Prepared by Sintering. *Appl. Mech. Mater.* **2011**, *71–78*, 3741–3744. [CrossRef]

50. Tan, G.; Shi, F.; Hao, S.; Chi, H.; Bailey, T.P.; Zhao, L.D.; Uher, C.; Wolverton, C.; Dravid, V.P.; Kanatzidis, M.G. Valence Band Modification and High Thermoelectric Performance in SnTe Heavily Alloyed with MnTe. *J. Am. Chem. Soc.* **2015**, *137*, 11507–11516. [CrossRef] [PubMed]

51. Hébert, S.; Daou, R.; Maignan, A.; Das, S.; Banerjee, A.; Klein, Y.; Bourgès, C.; Tsujii, N.; Mori, T. Thermoelectric Materials Taking Advantage of Spin Entropy: Lessons from Chalcogenides and Oxides. *Sci. Technol. Adv. Mater.* **2021**, *22*, 583–596. [CrossRef] [PubMed]

52. Xing, L.; Cui, W.; Sang, X.; Hu, F.; Wei, P.; Zhu, W.; Nie, X.; Zhang, Q.; Zhao, W. Enhanced Thermoelectric Performance and Atomic-Resolution Interfacial Structures in BiSbTe Thermo-Electro-Magnetic Nanocomposites Incorporating Magnetocaloric LaFeSi Nanoparticles. *J. Mater.* **2021**, *7*, 998–1006. [CrossRef]

53. Ioffe, A.F.; Stil'bans, L.S.; Iordanishvili, E.K.; Stavitskaya, T.S.; Gelbtuch, A.; Vineyard, G. Semiconductor Thermoelements and Thermoelectric Cooling. *Phys. Today* **1959**, *12*, 42. [CrossRef]

54. Popescu, A.; Woods, L.M.; Martin, J.; Nolas, G.S. Model of Transport Properties of Thermoelectric Nanocomposite Materials. *Phys. Rev. B* **2009**, *79*, 205302. [CrossRef]

55. Medlin, D.L.; Snyder, G.J. Interfaces in Bulk Thermoelectric Materials: A Review for Current Opinion in Colloid and Interface Science. *Curr. Opin. Colloid Interface Sci.* **2009**, *14*, 226–235. [CrossRef]

56. Heremans, J.P.; Thrush, C.M.; Morelli, D.T. Thermopower Enhancement in Lead Telluride Nanostructures. *Phys. Rev. B* **2004**, *70*, 115334. [CrossRef]

57. Kishimoto, K.; Yamamoto, K.; Koyanagi, T. Influences of Potential Barrier Scattering on the Thermoelectric, Properties of Sintered n-Type PbTe with a Small Grain Size. *Jpn. J. Appl. Phys.* **2003**, *42*, 501–508. [CrossRef]

58. Hu, Q.J.; Zhang, Y.; Zhang, Y.W.; Li, X.J.; Song, H.Z. High Thermoelectric Performance in Cu_2Se/CDs Hybrid Materials. *J. Alloy. Compd.* **2020**, *813*, 152204. [CrossRef]

59. Shakouri, A.; Lee, E.Y.; Smith, D.L.; Narayanamurti, V.; Bowers, J. Thermoelectric Effects in Submicron Heterostructure Barriers. *Microscale Thermophys. Eng.* **1998**, *2*, 37–47. [CrossRef]

60. Bahk, J.-H.; Bian, Z.X.; Shakouri, A. Electron Energy Filtering by a Nonplanar Potential to Enhance the Thermoelectric Power Factor in Bulk Materials. *Phys. Rev. B* **2013**, *87*, 075204. [CrossRef]

61. Rowe, D.M.; Min, G. Multiple Potential Barriers as a Possible Mechanism to Increase the Seebeck Coefficient and Electrical Power Factor. *AIP Conf. Proc.* **1994**, *316*, 339–342.

62. Whitlow, L.W.; Hirano, T. Superlattice Applications to Thermoelectricity. *J. Appl. Phys.* **1995**, *78*, 5460–5466. [CrossRef]

63. Zianni, X.; Narducci, D. Parametric Modeling of Energy Filtering by Energy Barriers in Thermoelectric Nanocomposites. *J. Appl. Phys.* **2015**, *117*, 035102. [CrossRef]

64. Ziman, J.M. *Electrons and Phonons: The Theory of Transport Phenomena in Solids*; Oxford University Press: Oxford, UK, 2001; ISBN 978-0-19-170993-7.

65. Jeong, C.; Kim, R.; Luisier, M.; Datta, S.; Lundstrom, M. On Landauer versus Boltzmann and Full Band versus Effective Mass Evaluation of Thermoelectric Transport Coefficients. *J. Appl. Phys.* **2010**, *107*, 023707. [CrossRef]

66. Faleev, S.V.; Leonard, F. Theory of Enhancement of Thermoelectric Properties of Materials with Nanoinclusions. *Phys. Rev. B* **2008**, *77*, 214304. [CrossRef]

67. Gayner, C.; Amouyal, Y. Energy Filtering of Charge Carriers: Current Trends, Challenges, and Prospects for Thermoelectric Materials. *Adv. Funct. Mater.* **2019**, *30*, 1901789. [CrossRef]

68. Singha, A.; Muralidharan, B. Incoherent Scattering Can Favorably Influence Energy Filtering in Nanostructured Thermoelectrics. *Sci. Rep.* **2017**, *7*, 7879. [CrossRef] [PubMed]

69. Narducci, D.; Selezneva, E.; Cerofolini, G.; Frabboni, S.; Ottaviani, G. Impact of Energy Filtering and Carrier Localization on the Thermoelectric Properties of Granular Semiconductors. *J. Solid State Chem.* **2012**, *193*, 19–25. [CrossRef]

70. Zhang, D.; Lei, J.; Guan, W.; Ma, Z.; Wang, C.; Zhang, L.; Cheng, Z.; Wang, Y. Enhanced Thermoelectric Performance of BiSbTe Alloy: Energy Filtering Effect of Nanoprecipitates and the Effect of SiC Nanoparticles. *J. Alloys Compd.* **2019**, *784*, 1276–1283. [CrossRef]

71. Liu, S.Q.; Kong, J.H.; Chen, H.M.; He, C.B. Interfacial Energy Barrier Tuning for Enhanced Thermoelectric Performance of PEDOT Nanowire/SWNT/PEDOT:PSS Ternary Composites. *ACS Appl. Energy Mater.* **2019**, *2*, 8843–8850. [CrossRef]

72. Jiang, X.Y.; Zhang, Q.K.; Deng, S.P.; Zhou, B.; Wang, B.; Chen, Z.Q.; Qi, N.; Tang, X.F. Enhanced Thermoelectric Performance of Polythiophene/Carbon Nanotube-Based Composites. *J. Electron. Mater.* **2020**, *49*, 2371–2380. [CrossRef]

73. An, H.; Pusko, M.; Chun, D.; Park, S.; Moon, J. In-Situ Synthesis of Flexible Hybrid Composite Films for Improved Thermoelectric Performance. *Chem. Eng. J.* **2019**, *357*, 547–558. [CrossRef]

74. Zhang, Z.; Zhao, W.; Zhu, W.; Ma, S.; Li, C.; Mu, X.; Wei, P.; Nie, X.; Zhang, Q.; Zhao, W. Preparation and Thermoelectric Performance of $BaTiO_3/Bi_{0.5}Sb_{1.5}Te_3$ Composite Materials. *J. Electron. Mater.* **2020**, *49*, 2794–2801. [CrossRef]

75. Jiang, Q.; Li, S.; Luo, Y.; Xin, J.; Li, S.; Li, W.; Zhao, G.; Yang, J. Ecofriendly Highly Robust Ag_8SiSe_6-Based Thermoelectric Composites with Excellent Performance Near Room Temperature. *ACS Appl. Mater. Interfaces* **2020**, *12*, 54653–54661. [CrossRef] [PubMed]

76. Cho, H.; Back, S.Y.; Yun, J.H.; Byeon, S.; Jin, H.; Rhyee, J.S. Thermoelectric Properties and Low-Energy Carrier Filtering by Mo Microparticle Dispersion in an n-Type $(CuI)_{0.003}Bi_2(Te,Se)_3$ Bulk Matrix. *ACS Appl. Mater. Interfaces* **2020**, *12*, 38076–38084. [CrossRef] [PubMed]

77. Li, X.X.; Yu, Z.K.; Zhou, H.B.; Yang, F.; Zhong, F.; Mao, X.H.; Li, B.Z.; Xin, H.; Gao, C.M.; Wang, L. Promoting the Thermoelectric Performance of Single-Walled Carbon Nanotubes by Inserting Discotic Liquid-Crystal Molecules. *ACS Sustain. Chem. Eng.* **2021**, *9*, 1891–1898. [CrossRef]

78. Davies, J.H. *The Physics of Low-Dimensional Semiconductors: An Introduction*, 1st ed.; Cambridge University Press: Cambridge, UK, 1997; ISBN 978-0-521-48148-9.

79. Liu, Y.; Guo, J.; Zhu, E.; Liao, L.; Lee, S.J.; Ding, M.; Shakir, I.; Gambin, V.; Huang, Y.; Duan, X. Approaching the Schottky-Mott Limit in van Der Waals Metal-Semiconductor Junctions. *Nature* **2018**, *557*, 696–700. [CrossRef]

80. Vashaee, D.; Shakouri, A. Improved Thermoelectric Power Factor in Metal-Based Superlattices. *Phys. Rev. Lett.* **2004**, *92*, 106103. [CrossRef]

81. Liu, M.; Qin, X.Y. Enhanced Thermoelectric Performance through Energy-Filtering Effects in Nanocomposites Dispersed with Metallic Particles. *Appl. Phys. Lett.* **2012**, *101*, 132103. [CrossRef]

82. Heremans, J.P.; Thrush, C.M.; Morelli, D.T. Thermopower Enhancement in PbTe with Pb Precipitates. *J. Appl. Phys.* **2005**, *98*, 063703. [CrossRef]

83. Ko, D.K.; Kang, Y.; Murray, C.B. Enhanced Thermopower via Carrier Energy Filtering in Solution-Processable $Pt-Sb_2Te_3$ Nanocomposites. *Nano Lett.* **2011**, *11*, 2841–2844. [CrossRef]

84. Zhou, Y.; Zhang, M.Y.; Liang, S. Improved Thermoelectric Performance of Cu_2O-Cr/Sn Composite Powder. *Chem. Phys. Lett.* **2021**, *777*, 138722. [CrossRef]

85. Gao, L.; Wang, S.; Liu, R.; Zha, X.; Sun, N.; Wang, S.; Wang, J.; Fu, G. Enhanced Thermoelectric Performance of CdO: Ag Nanocomposites. *Dalton Trans.* **2016**, *45*, 12215–12220. [CrossRef] [PubMed]

86. Milnes, A.G.; Feucht, D.L. *Heterojunctions and Metal Semiconductor Junctions*; Elsevier: Amsterdam, The Netherlands, 1972; ISBN 978-0-12-498050-1.

87. Mayergoyz, I.D. Solution of the Nonlinear Poisson Equation of Semiconductor Device Theory. *J. Appl. Phys.* **1986**, *59*, 195–199. [CrossRef]

88. Wu, H.J.; Carrete, J.; Zhang, Z.Y.; Qu, Y.Q.; Shen, X.T.; Wang, Z.; Zhao, L.D.; He, J.Q. Strong Enhancement of Phonon Scattering through Nanoscale Grains in Lead Sulfide Thermoelectrics. *NPG Asia Mater.* **2014**, *6*, e108. [CrossRef]

89. Seto, J.Y.W. The Electrical Properties of Polycrystalline Silicon Films. *J. Appl. Phys.* **1975**, *46*, 5247–5254. [CrossRef]

90. Taylor, W.E.; Odell, N.H.; Fan, H.Y. Grain Boundary Barriers in Germanium. *Phys. Rev.* **1952**, *88*, 867–875. [CrossRef]

91. Zhou, Z.W.; Yang, J.Y.; Jiang, Q.H.; Zhang, D.; Xin, J.W.; Li, X.; Ren, Y.Y.; He, X. Thermoelectric Performance of SnTe with ZnO Carrier Compensation, Energy Filtering, and Multiscale Phonon Scattering. *J. Am. Ceram. Soc.* **2017**, *100*, 5723–5730. [CrossRef]

92. Dou, Y.C.; Qin, X.Y.; Li, D.; Li, L.L.; Zou, T.H.; Wang, Q.Q. Enhanced Thermopower and Thermoelectric Performance through Energy Filtering of Carriers in $(Bi_2Te_3)_{(0.2)}(Sb_2Te_3)_{(0.8)}$ Bulk Alloy Embedded with Amorphous SiO_2 Nanoparticles. *J. Appl. Phys.* **2013**, *114*, 7. [CrossRef]

93. Fang, T.; Li, X.; Hu, C.; Zhang, Q.; Yang, J.; Zhang, W.; Zhao, X.; Singh, D.J.; Zhu, T. Complex Band Structures and Lattice Dynamics of Bi_2Te_3-Based Compounds and Solid Solutions. *Adv. Funct. Mater.* **2019**, *29*, 1900677. [CrossRef]

94. Li, Y.; Dou, Y.; Qin, X.; Zhang, J.; Xin, H.; Li, D.; Song, C.; Zou, T.; Liu, Y.; Li, C. Enhanced Thermoelectric Figure of Merit in P-Type $\beta-Zn_4Sb_3/Bi_{0.4}Sb_{1.6}Te_3$ Nanocomposites. *RSC Adv.* **2016**, *6*, 12243–12248. [CrossRef]

95. Nguyen, T.H.; Enju, J.; Ono, T. Enhancement of Thermoelectric Properties of Bismuth Telluride Composite with Gold Nano-Particles Inclusions Using Electrochemical Co-Deposition. *J. Electrochem. Soc.* **2019**, *166*, D508. [CrossRef]

96. Madavali, B.; Kim, H.S.; Lee, K.H.; Hong, S.J. Enhanced Seebeck Coefficient by Energy Filtering in Bi-Sb-Te Based Composites with Dispersed Y_2O_3 Nanoparticles. *Intermetallics* **2017**, *82*, 68–75. [CrossRef]

97. Ravich, I.I. *Semiconducting Lead Chalcogenide*; Monographs in Semiconductor Physics; Springer: New York, NY, USA, 1970; ISBN 978-1-4684-8609-4.

98. Zou, T.; Qin, X.; Zhang, Y.; Li, X.; Zeng, Z.; Li, D.; Zhang, J.; Xin, H.; Xie, W.; Weidenkaff, A. Enhanced Thermoelectric Performance of β-Zn_4Sb_3 Based Nanocomposites through Combined Effects of Density of States Resonance and Carrier Energy Filtering. *Sci. Rep.* **2015**, *5*, 17803. [CrossRef] [PubMed]

99. Xiong, Z.; Chen, X.; Zhao, X.; Bai, S.; Huang, X.; Chen, L. Effects of Nano-TiO_2 Dispersion on the Thermoelectric Properties Offilled-Skutterudite $Ba_{0.22}Co_4Sb_{12}$. *Solid State Sci.* **2009**, *11*, 1612–1616. [CrossRef]

100. Dette, C.; Perez-Osorio, M.A.; Kley, C.S.; Punke, P.; Patrick, C.E.; Jacobson, P.; Giustino, F.; Jung, S.J.; Kern, K. TiO_2 Anatase with a Bandgap in the Visible Region. *Nano Lett.* **2014**, *14*, 6533–6538. [CrossRef]

101. Yang, Y.-X.; Wu, Y.-H.; Zhang, Q.; Cao, G.-S.; Zhu, T.-J.; Zhao, X.-B. Enhanced Thermoelectric Performance of Bi_2Se_3/TiO_2 Composite. *Rare Met.* **2020**, *39*, 887–894. [CrossRef]

102. Ou, C.; Hou, J.; Wei, T.-R.; Jiang, B.; Jiao, S.; Li, J.-F.; Zhu, H. High Thermoelectric Performance of All-Oxide Heterostructures with Carrier Double-Barrier Filtering Effect. *NPG Asia Mater.* **2015**, *7*, e182. [CrossRef]

103. Yang, X.; Chen, S.; Zhang, H.; Lv, F.; Fan, W.; Wang, W.; Munir, Z.A. Thermoelectric Properties and Transport Mechanism of Pure and Bi-Doped SiNWs-Mg_2Si. *Phys. Status Solidi A Appl. Mater. Sci.* **2018**, *215*, 1700742. [CrossRef]

104. Hu, Q.; Wang, K.; Zhang, Y.; Li, X.; Song, H. Enhanced Thermoelectric Properties of Nano SiC Dispersed $Bi_2Sr_2Co_2Oy$ Ceramics. *Mater. Res. Express* **2018**, *5*, 045510. [CrossRef]

105. Zhou, Z.; Li, J.; Fan, Y.; Zhang, Q.; Lu, X.; Fan, S.; Kikuchi, K.; Nomura, N.; Kawasaki, A.; Wang, L.; et al. Uniform Dispersion of SiC in Yb-Filled Skutterudite Nanocomposites with High Thermoelectric and Mechanical Performance. *Scr. Mater.* **2019**, *162*, 166–171. [CrossRef]

106. Zhang, W.; Zhu, K.; Liu, J.; Wang, J.; Yan, K.; Liu, P.; Wang, Y. Enhanced Thermoelectric Properties of Nano-SiC Dispersed $NaCo_2O_4$ Composites. *Funct. Mater. Lett.* **2019**, *12*, 1950009. [CrossRef]

107. Xia, Y.; Park, J.; Zhou, F.; Ozoliņš, V. High Thermoelectric Power Factor in Intermetallic CoSi Arising from Energy Filtering of Electrons by Phonon Scattering. *Phys. Rev. Appl.* **2019**, *11*, 024017. [CrossRef]

108. Ahmad, S.; Basu, R.; Sarkar, P.; Singh, A.; Bohra, A.; Bhattacharya, S.; Bhatt, R.; Meshram, K.N.; Samanta, S.; Bhatt, P.; et al. Enhanced Thermoelectric Figure-of-Merit of p-Type SiGe through TiO_2 Nanoinclusions and Modulation Doping of Boron. *Materialia* **2018**, *4*, 147–156. [CrossRef]

109. Felizco, J.C.; Uenuma, M.; Fujii, M.N.; Uraoka, Y. Improved Thermoelectric Power Factor of InGaZnO/SiO Thin Film Transistor via Gate-Tunable Energy Filtering. *IEEE Electron Device Lett.* **2021**, *42*, 1236–1239. [CrossRef]

110. Solá, F.; Dynys, F.W. Probing the Mechanical Properties and Microstructure of WSi2/SixGe1−x Multiphase Thermoelectric Material by Nanoindentation, Electron and Focused Ion Beam Microscopy Methods. *J. Alloy. Compd.* **2015**, *633*, 165–169. [CrossRef]

111. Neophytou, N.; Zianni, X.; Kosina, H.; Frabboni, S.; Lorenzi, B.; Narducci, D. Simultaneous Increase in Electrical Conductivity and Seebeck Coefficient in Highly Boron-Doped Nanocrystalline Si. *Nanotechnology* **2013**, *24*, 205402. [CrossRef] [PubMed]

112. Kang, H.B.; Poudel, B.; Li, W.; Lee, H.; Saparamadu, U.; Nozariasbmarz, A.; Kang, M.G.; Gupta, A.; Heremans, J.J.; Priya, S. Decoupled Phononic-Electronic Transport in Multi-Phase n-Type Half-Heusler Nanocomposites Enabling Efficient High Temperature Power Generation. *Mater. Today* **2020**, *36*, 63–72. [CrossRef]

113. Pakdel, A.; Guo, Q.; Nicolosi, V.; Mori, T. Enhanced Thermoelectric Performance of Bi-Sb-Te/Sb_2O_3 Nanocomposites by Energy Filtering Effect. *J. Mater. Chem. A* **2018**, *6*, 21341–21349. [CrossRef]

114. Li, S.; Liu, Y.; Liu, F.; He, D.; He, J.; Luo, J.; Xiao, Y.; Pan, F. Effective Atomic Interface Engineering in $Bi_2Te_{2.7}Se_{0.3}$ Thermoelectric Material by Atomic-Layer-Deposition Approach. *Nano Energy* **2018**, *49*, 257–266. [CrossRef]

115. Güneş, E.; Wickleder, M.S.; Müller, E.; Elm, M.T.; Klar, P.J. Improved Thermoelectric Properties of Nanostructured Composites out of $Bi_{1−x}Sb_x$ Nanoparticles and Carbon Phases. *AIP Adv.* **2018**, *8*, 075319. [CrossRef]

116. Wang, Y.S.; Huang, L.L.; Li, D.; Zhang, J.; Qin, X.Y. Enhanced Thermoelectric Performance of $Bi_{0.4}Sb_{1.6}Te_3$ Based Composites with $CuInTe_2$ Inclusions. *J. Alloys Compd.* **2018**, *758*, 72–77. [CrossRef]

117. Cao, R.; Zhu, Z.; Li, X.-J.; Hu, X.; Song, H. Enhanced Thermoelectric Properties of the Lu-Doped and CNT-Dispersed Bi_2Te_3 Alloy. *Appl. Phys. A Mater. Sci. Process.* **2019**, *125*. [CrossRef]

118. Wan, X.; Liu, Z.; Sun, L.; Jiang, P.; Bao, X. Synergetic Enhancement of Thermoelectric Performance in a $Bi_{0.5}Sb_{1.5}Te_3$/$SrTiO_3$ Heterostructure. *J. Mater. Chem. A* **2020**, *8*, 10839–10844. [CrossRef]

119. Park, N.-W.; Lee, W.-Y.; Yoon, Y.-S.; Kim, G.-S.; Yoon, Y.-G.; Lee, S.-K. Achieving Out-of-Plane Thermoelectric Figure of Merit ZT = 1.44 in a p-Type Bi_2Te_3/$Bi_{0.5}Sb_{1.5}Te_3$ Superlattice Film with Low Interfacial Resistance. *ACS Appl. Mater. Interfaces* **2019**, *11*, 38247–38254. [CrossRef] [PubMed]

120. Li, Y.; Wang, X.; Liu, G.; Shin, B.; Shan, F. High Thermoelectric Efficiency of P-Type BiSbTe-Based Composites with $CuGaTe_2$ Nanoinclusions. *Scr. Mater.* **2019**, *172*, 88–92. [CrossRef]

121. Lwin, M.L.; Dharmaiah, P.; Min, B.H.; Song, G.; Jung, K.Y.; Hong, S.-J. Tuning of Thermoelectric Transport Properties via the Formation of Hierarchical Structures in Bi-Doped Gd_2O_3/$Bi_{0.5}Sb_{1.5}Te_3$ Nanocomposites. *Int. J. Energy Res.* **2021**. [CrossRef]

122. Ahmad, M.; Kodan, N.; Ghosh, A.; Mehta, B.R. The Nature of 2D:3D SnS:Bi$_2$Te$_3$ Interface and Its Effect on Enhanced Electrical and Thermoelectric Properties. *J. Alloy. Compd.* **2020**, *847*, 156233. [CrossRef]

123. Zhao, L.; Qiu, W.; Sun, Y.; Chen, L.; Deng, H.; Yang, L.; Shi, X.; Tang, J. Enhanced Thermoelectric Performance of Bi$_{0.3}$Sb$_{1.7}$Te$_3$ Based Alloys by Dispersing TiC Ceramic Nanoparticles. *J. Alloy. Compd.* **2021**, *863*, 158376. [CrossRef]

124. Zhang, Y.; Xing, C.; Liu, Y.; Li, M.; Xiao, K.; Guardia, P.; Lee, S.; Han, X.; Ostovari Moghaddam, A.; Josep Roa, J.; et al. Influence of Copper Telluride Nanodomains on the Transport Properties of N-Type Bismuth Telluride. *Chem. Eng. J.* **2021**, *418*, 129374. [CrossRef]

125. Hwang, J.; Lee, M.; Yu, B.-K.; Han, M.-K.; Kim, W.; Kim, J.; Al Rahal Al Orabi, R.; Wang, H.; Acharya, S.; Kim, J.; et al. Enhancement of Thermoelectric Performance in a Non-Toxic CuInTe$_2$/SnTe Coated Grain Nanocomposite. *J. Mater. Chem. A* **2021**, *9*, 14851–14858. [CrossRef]

126. Dharmaiah, P.; Nagarjuna, C.; Sharief, P.; Hong, S.-J. Synergetic Effects of Co-Dispersed Cu and Insulating HfO$_2$ Nanoparticles Enabled High Thermoelectric Figure of Merit in Bi$_{0.5}$Sb$_{1.5}$Te$_3$ Composites. *Appl. Surf. Sci.* **2021**, *556*, 149783. [CrossRef]

127. Pei, Y.L.; Wu, H.; Wu, D.; Zheng, F.; He, J. High Thermoelectric Performance Realized in a BiCuSeO System by Improving Carrier Mobility through 3D Modulation Doping. *J. Am. Chem. Soc.* **2014**, *136*, 13902–13908. [CrossRef]

128. Dingle, R.; Störmer, H.L.; Gossard, A.C.; Wiegmann, W. Electron Mobilities in Modulation-doped Semiconductor Heterojunction Superlattices. *Appl. Phys. Lett.* **1978**, *33*, 665–667. [CrossRef]

129. Mimura, T.; Hiyamizu, S.; Fujii, T.; Nanbu, K. A New Field-Effect Transistor with Selectively Doped GaAs/n-Al$_x$Ga$_{1-x}$As Heterojunctions. *Jpn. J. Appl. Phys.* **1980**, *19*, L225–L227. [CrossRef]

130. Pfeiffer, L.; West, K.W.; Stormer, H.L.; Baldwin, K.W. Electron Mobilities Exceeding 10^7 cm^2/V s in Modulation-doped GaAs. *Appl. Phys. Lett.* **1998**, *55*, 1888. [CrossRef]

131. Yamini, S.A.; Mitchell, D.R.G.; Gibbs, Z.M.; Santos, R.; Patterson, V.; Li, S.; Pei, Y.Z.; Dou, S.X.; Snyder, G.J. Heterogeneous Distribution of Sodium for High Thermoelectric Performance of P-Type Multiphase Lead-Chalcogenides. *Adv. Energy Mater.* **2015**, *5*, 1501047. [CrossRef]

132. Tian, Y.; Sakr, M.R.; Kinder, J.M.; Liang, D.; MacDonald, M.J.; Qiu, R.L.J.; Gao, H.-J.; Gao, X.P.A. One-Dimensional Quantum Confinement Effect Modulated Thermoelectric Properties in InAs Nanowires. *Nano Lett.* **2012**, *12*, 6492–6497. [CrossRef] [PubMed]

133. Moon, J.; Kim, J.-H.; Chen, Z.C.Y.; Xiang, J.; Chen, R. Gate-Modulated Thermoelectric Power Factor of Hole Gas in Ge-Si Core-Shell Nanowires. *Nano Lett.* **2013**, *13*, 1196–1202. [CrossRef]

134. Liang, W.; Hochbaum, A.I.; Fardy, M.; Rabin, O.; Zhang, M.; Yang, P. Field-Effect Modulation of Seebeck Coefficient in Single PbSe Nanowires. *Nano Lett.* **2009**, *9*, 1689–1693. [CrossRef] [PubMed]

135. Curtin, B.M.; Codecido, E.A.; Krämer, S.; Bowers, J.E. Field-Effect Modulation of Thermoelectric Properties in Multigated Silicon Nanowires. *Nano Lett.* **2013**, *13*, 5503–5508. [CrossRef] [PubMed]

136. Neophytou, N.; Thesberg, M. Modulation Doping and Energy Filtering as Effective Ways to Improve the Thermoelectric Power Factor. *J. Comput. Electron.* **2016**, *15*, 16–26. [CrossRef]

137. Zhang, Y.; Brorsson, J.; Qiu, R.; Palmqvist, A.E.C. Enhanced Thermoelectric Performance of Ba$_8$Ga$_{16}$Ge$_{30}$ Clathrate by Modulation Doping and Improved Carrier Mobility. *Adv. Electron. Mater.* **2021**, *7*, 2000782. [CrossRef]

138. Rathore, E.; Guin, S.N.; Biswas, K. Enhancement of Thermoelectric Performance of N-Type AgBi$_{1+x}$Se$_2$ via Improvement of the Carrier Mobility by Modulation Doping. *Bull. Mater. Sci.* **2020**, *43*, 315. [CrossRef]

139. Peng, Y.; Lai, H.; Liu, C.; Gao, J.; Kurosawa, M.; Nakatsuka, O.; Takeuchi, T.; Zaima, S.; Tanemura, S.; Miao, L. Realizing High Thermoelectric Performance in P-Type Si$_{1-x}$-YGexSny Thin Films at Ambient Temperature by Sn Modulation Doping. *Appl. Phys. Lett.* **2020**, *117*, 053903. [CrossRef]

140. Souda, D.; Shimizu, K.; Ohishi, Y.; Muta, H.; Yagi, T.; Kurosaki, K. High Thermoelectric Power Factor of Si–Mg$_2$Si Nanocomposite Ribbons Synthesized by Melt Spinning. *ACS Appl. Energy Mater.* **2020**, *3*, 1962–1968. [CrossRef]

141. Lee, D.; Zhou, J.; Chen, G.; Shao-Horn, Y. Enhanced Thermoelectric Properties for PEDOT:PSS/Undoped Ge Thin-Film Bilayered Heterostructures. *Adv. Electron. Mater.* **2019**, *5*, 1800624. [CrossRef]

142. Hui, S.; Gao, W.; Lu, X.; Panda, A.; Bailey, T.P.; Page, A.A.; Forrest, S.R.; Morelli, D.T.; Pan, X.; Pipe, K.P.; et al. Engineering Temperature-Dependent Carrier Concentration in Bulk Composite Materials via Temperature-Dependent Fermi Level Offset. *Adv. Energy Mater.* **2017**, *8*, 1701623. [CrossRef]

143. Feng, B.; Li, G.; Pan, Z.; Hu, X.; Liu, P.; He, Z.; Li, Y.; Fan, X. Enhanced Thermoelectric Properties in BiCuSeO Ceramics by Pb/Ni Dual Doping and 3D Modulation Doping. *J. Solid State Chem.* **2019**, *271*, 1–7. [CrossRef]

144. Feng, B.; Li, G.; Pan, Z.; Hu, X.; Liu, P.; Li, Y.; He, Z.; Fan, X. Enhanced Thermoelectric Performances in BiCuSeO Oxyselenides via Er and 3D Modulation Doping. *Ceram. Int.* **2019**, *45*, 4493–4498. [CrossRef]

145. Feng, B.; Li, G.; Pan, Z.; Hu, X.; Liu, P.; He, Z.; Li, Y.; Fan, X. Enhanced Thermoelectric Performance in BiCuSeO Oxyselenides via Ba/Te Dual-Site Substitution and 3D Modulation Doping. *J. Solid State Chem.* **2018**, *266*, 297–303. [CrossRef]

146. Wu, D.; Zhao, L.-D.; Tong, X.; Li, W.; Wu, L.; Tan, Q.; Pei, Y.; Huang, L.; Li, J.-F.; Zhu, Y.; et al. Superior Thermoelectric Performance in PbTe–PbS Pseudo-Binary: Extremely Low Thermal Conductivity and Modulated Carrier Concentration. *Energy Environ. Sci.* **2015**, *8*, 2056–2068. [CrossRef]

147. Rowe, D.M. (Ed.) *Thermoelectrics Handbook*, 1st ed.; CRC Press: Boca Raton, FL, USA, 2006; ISBN 978-1-4200-3890-3.

148. Hong, M.; Wang, Y.; Feng, T.; Sun, Q.; Xu, S.; Matsumura, S.; Pantelides, S.T.; Zou, J.; Chen, Z.G. Strong Phonon-Phonon Interactions Securing Extraordinary Thermoelectric Ge1- XSb XTe with Zn-Alloying-Induced Band Alignment. *J. Am. Chem. Soc.* **2019**, *141*, 1742–1748. [CrossRef]

149. Bao, D.Y.; Chen, J.; Yu, Y.; Liu, W.D.; Huang, L.S.; Han, G.; Tang, J.; Zhou, D.L.; Yang, L.; Chen, Z.G. Texture-Dependent Thermoelectric Properties of Nano-Structured Bi_2Te_3. *Chem. Eng. J.* **2020**, *388*, 124295. [CrossRef]

150. Alam, H.; Ramakrishna, S. A Review on the Enhancement of Figure of Merit from Bulk to Nano-Thermoelectric Materials. *Nano Energy* **2013**, *2*, 190–212. [CrossRef]

151. Dresselhaus, M.S.; Chen, G.; Tang, M.Y.; Yang, R.G.; Lee, H.; Wang, D.Z.; Ren, Z.F.; Fleurial, J.P.; Gogna, P. New Directions for Low-Dimensional Thermoelectric Materials. *Adv. Mater.* **2007**, *19*, 1043–1053. [CrossRef]

152. Chen, X.; Parker, D.; Singh, D.J. Acoustic Impedance and Interface Phonon Scattering in Bi_2Te_3 and Other Semiconducting Materials. *Phys. Rev. B* **2013**, *87*, 045317. [CrossRef]

153. Yang, J.; Meisner, G.P.; Chen, L. Strain Field Fluctuation Effects on Lattice Thermal Conductivity of ZrNiSn-Based Thermoelectric Compounds. *Appl. Phys. Lett.* **2004**, *85*, 1140–1142. [CrossRef]

154. Yan, X.; Liu, W.S.; Wang, H.; Chen, S.; Shiomi, J.; Esfarjani, K.; Wang, H.Z.; Wang, D.Z.; Chen, G.; Ren, Z.F. Stronger Phonon Scattering by Larger Differences in Atomic Mass and Size in P-Type Half-Heuslers Hf1-XTixCoSb$_{0.8}$Sn$_{0.2}$. *Energy Environ. Sci.* **2012**, *5*, 7543–7548. [CrossRef]

155. Xie, H.; Wang, H.; Fu, C.; Liu, Y.; Snyder, G.J.; Zhao, X.; Zhu, T. The Intrinsic Disorder Related Alloy Scattering in ZrNiSn Half-Heusler Thermoelectric Materials. *Sci. Rep.* **2014**, *4*, 6888. [CrossRef] [PubMed]

156. Bhattacharya, S.; Skove, M.J.; Russell, M.; Tritt, T.M.; Xia, Y.; Ponnambalam, V.; Poon, S.J.; Thadhani, N. Effect of Boundary Scattering on the Thermal Conductivity of TiNiSn-Based Half-Heusler Alloys. *Phys. Rev. B* **2008**, *77*, 184203. [CrossRef]

157. Bhattacharya, S.; Tritt, T.M.; Xia, Y.; Ponnambalam, V.; Poon, S.J.; Thadhani, N. Grain Structure Effects on the Lattice Thermal Conductivity of Ti-Based Half-Heusler Alloys. *Appl. Phys. Lett.* **2002**, *81*, 43–45. [CrossRef]

158. Yan, X.; Joshi, G.; Liu, W.; Lan, Y.; Wang, H.; Lee, S.; Simonson, J.W.; Poon, S.J.; Tritt, T.M.; Chen, G.; et al. Enhanced Thermoelectric Figure of Merit of P-Type Half-Heuslers. *Nano Lett.* **2011**, *11*, 556–560. [CrossRef]

159. Joshi, G.; Yan, X.; Wang, H.; Liu, W.; Chen, G.; Ren, Z. Enhancement in Thermoelectric Figure-Of-Merit of an N-Type Half-Heusler Compound by the Nanocomposite Approach. *Adv. Energy Mater.* **2011**, *1*, 643–647. [CrossRef]

160. Jiang, P.; Lindsay, L.; Huang, X.; Koh, Y.K. Interfacial Phonon Scattering and Transmission Loss in >1 Mm Thick Silicon-on-Insulator Thin Films. *Phys. Rev. B* **2018**, *97*, 195308. [CrossRef]

161. Klemens, P.G.; Simon, F.E. The Thermal Conductivity of Dielectric Solids at Low Temperatures (Theoretical). *Proc. R. Soc. Lond. Ser. A Math. Phys. Sci.* **1951**, *208*, 108–133. [CrossRef]

162. Holland, M.G. Analysis of Lattice Thermal Conductivity. *Phys. Rev.* **1963**, *132*, 2461–2471. [CrossRef]

163. Callaway, J. Model for Lattice Thermal Conductivity at Low Temperatures. *Phys. Rev.* **1959**, *113*, 1046–1051. [CrossRef]

164. Limarga, A.M.; Shian, S.; Leckie, R.M.; Levi, C.G.; Clarke, D.R. Thermal Conductivity of Single- and Multi-Phase Compositions in the ZrO_2-Y_2O_3-Ta_2O_5 System. *J. Eur. Ceram. Soc.* **2014**, *34*, 3085–3094. [CrossRef]

165. Zhao, H.Z.; Pokheral, M.; Zhu, G.H.; Chen, S.; Lukas, K.; Jie, Q.; Opeil, C.; Chen, G.; Ren, Z.F. Dramatic Thermal Conductivity Reduction by Nanostructures for Large Increase in Thermoelectric Figure-of-Merit of $FeSb_2$. *Appl. Phys. Lett.* **2011**, *99*, 163101. [CrossRef]

166. Gurunathan, R.; Hanus, R.; Jeffrey Snyder, G. Alloy Scattering of Phonons. *Mater. Horiz.* **2020**, *7*, 1452–1456. [CrossRef]

167. Nan, C.-W.; Birringer, R. Determining the Kapitza Resistance and the Thermal Conductivity of Polycrystals: A Simple Model. *Phys. Rev. B* **1998**, *57*, 8264–8268. [CrossRef]

168. Kinsler, L.E.; Frey, A.R.; Coppens, A.B.; Sanders, J.V. *Fundamentals of Acoustics*, 4th ed.; Wiley: Hoboken, NJ, USA, 1999.

169. James, D.; Lu, X.; Nguyen, A.C.; Morelli, D.; Brock, S.L. Design of Lead Telluride Based Thermoelectric Materials through Incorporation of Lead Sulfide Inclusions or Ligand Stripping of Nanosized Building Blocks. *J. Phys. Chem. C* **2015**, *119*, 4635–4644. [CrossRef]

170. Ahmad, K.; Almutairi, Z.; Wan, C. Thermoelectric Properties of PbTe-Based Graphene Nanocomposite. *J. Mater. Sci. Mater. Electron.* **2020**, *31*, 20996–21004. [CrossRef]

171. Aminorroaya Yamini, S.; Wang, H.; Gibbs, Z.M.; Pei, Y.; Mitchell, D.R.G.; Dou, S.X.; Snyder, G.J. Thermoelectric Performance of Tellurium-Reduced Quaternary p-Type Lead–Chalcogenide Composites. *Acta Mater.* **2014**, *80*, 365–372. [CrossRef]

172. Falkenbach, O.; Hartung, D.; Klar, P.J.; Koch, G.; Schlecht, S. Thermoelectric Properties of Nanostructured Bismuth-Doped Lead Telluride $Bi_x(PbTe)_{1-x}$ Prepared by Co-Ball-Milling. *J. Electron. Mater.* **2013**, *43*, 1674–1680. [CrossRef]

173. Falkenbach, O.; Schmitz, A.; Hartung, D.; Dankwort, T.; Koch, G.; Kienle, L.; Klar, P.J.; Mueller, E.; Schlecht, S. Effect of Preparation Procedure and Nanostructuring on the Thermoelectric Properties of the Lead Telluride-Based Material System AgPb$_m$BiTe$_{2+m}$ (BLST-m). *J. Appl. Phys.* **2016**, *119*, 214310. [CrossRef]

174. Keshavarz, M.K.; Vasilevskiy, D.; Masut, R.A.; Turenne, S. Synthesis and Characterization of Bismuth Telluride-Based Thermoelectric Nanocomposites Containing MoS_2 Nano-Inclusions. *Mater. Charact.* **2014**, *95*, 44–49. [CrossRef]

175. Trawiński, B.; Bochentyn, B.; Gostkowska, N.; Łapiński, M.; Miruszewski, T.; Kusz, B. Structure and Thermoelectric Properties of Bismuth Telluride—Carbon Composites. *Mater. Res. Bull.* **2018**, *99*, 10–17. [CrossRef]

176. Yang, G.; Sang, L.; Yun, F.F.; Mitchell, D.R.G.; Casillas, G.; Ye, N.; See, K.; Pei, J.; Wang, X.; Li, J.; et al. Significant Enhancement of Thermoelectric Figure of Merit in BiSbTe-Based Composites by Incorporating Carbon Microfiber. *Adv. Funct. Mater.* **2021**, *31*, 2008851. [CrossRef]

177. Zhang, J.; Wu, D.; He, D.; Feng, D.; Yin, M.; Qin, X.; He, J. Extraordinary Thermoelectric Performance Realized in N-Type PbTe through Multiphase Nanostructure Engineering. *Adv. Mater.* **2017**, *29*, 1703148. [CrossRef]

178. Sootsman, J.R.; He, J.Q.; Dravid, V.P.; Li, C.P.; Uher, C.; Kanatzidis, M.G. High Thermoelectric Figure of Merit and Improved Mechanical Properties in Melt Quenched PbTe-Ge and PbTe-Ge$_{1-x}$Si$_x$ Eutectic and Hypereutectic Composites. *J. Appl. Phys.* **2009**, *105*, 083718. [CrossRef]

179. Gaultois, M.W.; Sparks, T.D.; Borg, C.K.H.; Seshadri, R.; Bonificio, W.D.; Clarke, D.R. Data-Driven Review of Thermoelectric Materials: Performance and Resource Considerations. *Chem. Mater.* **2013**, *25*, 2911–2920. [CrossRef]

180. Gaultois, M.W.; Sparks, T.D.; Borg, C.K.H.; Seshadri, R.; Bonificio, W.D.; Clarke, D.R. Energy Materials Datamining. Available online: http://www.mrl.ucsb.edu:8080/datamine/about.jsp (accessed on 23 August 2021).

181. Kittel, C. *Introduction to Solid State Physics*, 8th ed.; John Wiley & Sons: New York, NY, USA, 2018; ISBN 978-1-119-45620-9.

182. Chung, D.Y.; Hogan, T.; Brazis, P.; Rocci-Lane, M.; Kannewurf, C.; Bastea, M.; Uher, C.; Kanatzidis, M.G. CsBi$_4$Te$_6$: A High-Performance Thermoelectric Material for Low-Temperature Applications. *Science* **2000**, *287*, 1024–1027. [CrossRef] [PubMed]

183. Chung, D.-Y.; Choi, K.-S.; Iordanidis, L.; Schindler, J.L.; Brazis, P.W.; Kannewurf, C.R.; Chen, B.; Hu, S.; Uher, C.; Kanatzidis, M.G. High Thermopower and Low Thermal Conductivity in Semiconducting Ternary K−Bi−Se Compounds. Synthesis and Properties of β-K$_2$Bi$_8$Se$_{13}$ and K$_{2.5}$Bi$_{8.5}$Se$_{14}$ and Their Sb Analogues. *Chem. Mater.* **1997**, *9*, 3060–3071. [CrossRef]

184. Gascoin, F.; Maignan, A. Order-Disorder Transition in AgCrSe$_2$: A New Route to Efficient Thermoelectrics. *Chem. Mater.* **2011**, *23*, 2510–2513. [CrossRef]

185. Hsu, K.F.; Loo, S.; Guo, F.; Chen, W.; Dyck, J.S.; Uher, C.; Hogan, T.; Polychroniadis, E.K.; Kanatzidis, M.G. Cubic AgPb$_{(m)}$SbTe$_{(2+m)}$: Bulk Thermoelectric Materials with High Figure of Merit. *Science* **2004**, *303*, 818–821. [CrossRef]

186. Jungwirth, T.; Wunderlich, J.; Olejník, K. Spin Hall Effect Devices. *Nat. Mater.* **2012**, *11*, 382–390. [CrossRef]

187. Kanatzidis, M.G.; McCarthy, T.J.; Tanzer, T.A.; Chen, L.-H.; Iordanidis, L.; Hogan, T.; Kannewurf, C.R.; Uher, C.; Chen, B. Synthesis and Thermoelectric Properties of the New Ternary Bismuth Sulfides KBi$_{6.33}$S$_{10}$ and K$_2$Bi$_8$S$_{13}$. *Chem. Mater.* **1996**, *8*, 1465–1474. [CrossRef]

188. Kurosaki, K.; Kosuga, A.; Yamanaka, S. Thermoelectric Properties of Chevrel Phase Mo6Te8-XSx. *J. Alloys Compd.* **2003**, *351*, 208–211. [CrossRef]

189. Kurosaki, K.; Kosuga, A.; Muta, H.; Uno, M.; Yamanaka, S. Ag$_9$TlTe$_5$: A High-Performance Thermoelectric Bulk Material with Extremely Low Thermal Conductivity. *Appl. Phys. Lett.* **2005**, *87*, 061919. [CrossRef]

190. Larouche, S.; Tsai, Y.J.; Tyler, T.; Jokerst, N.M.; Smith, D.R. Infrared Metamaterial Phase Holograms. *Nat. Mater.* **2012**, *11*, 450–454. [CrossRef] [PubMed]

191. Liu, H.; Shi, X.; Xu, F.; Zhang, L.; Zhang, W.; Chen, L.; Li, Q.; Uher, C.; Day, T.; Snyder, G.J. Copper Ion Liquid-like Thermoelectrics. *Nat. Mater.* **2012**, *11*, 422–425. [CrossRef] [PubMed]

192. Martin, C.D.; Costa, A.; Dering, B.; Hoshino, N.; Wu, Y.J.; Thierry, G. Effects of Speed of Word Processing on Semantic Access: The Case of Bilingualism. *Brain Lang.* **2012**, *120*, 61–65. [CrossRef]

193. May, A.F.; Flage-Larsen, E.; Snyder, G.J. Electron and Phonon Scattering in the High-Temperature Thermoelectric La$_3$Te$_{4-z}$M$_z$ (M = Sb,Bi). *Phys. Rev. B* **2010**, *81*, 125205. [CrossRef]

194. McGuire, M.A.; Reynolds, T.K.; DiSalvo, F.J. Exploring Thallium Compounds as Thermoelectric Materials: Seventeen New Thallium Chalcogenides. *Chem. Mater.* **2005**, *17*, 2875–2884. [CrossRef]

195. Ohta, M.; Yamamoto, A.; Obara, H. Thermoelectric Properties of Chevrel-Phase Sulfides M$_x$Mo$_6$S$_8$ (M: Cr, Mn, Fe, Ni). *J. Electron. Mater.* **2010**, *39*, 2117–2121. [CrossRef]

196. Orava, J.; Greer, A.L.; Gholipour, B.; Hewak, D.W.; Smith, C.E. Characterization of Supercooled Liquid Ge2Sb2Te5 and Its Crystallization by Ultrafast-Heating Calorimetry. *Nat. Mater.* **2012**, *11*, 279–283. [CrossRef] [PubMed]

197. Pei, Y.; Shi, X.; LaLonde, A.; Wang, H.; Chen, L.; Snyder, G.J. Convergence of Electronic Bands for High Performance Bulk Thermoelectrics. *Nature* **2011**, *473*, 66–69. [CrossRef] [PubMed]

198. Rogers, E.T.; Lindberg, J.; Roy, T.; Savo, S.; Chad, J.E.; Dennis, M.R.; Zheludev, N.I. A Super-Oscillatory Lens Optical Microscope for Subwavelength Imaging. *Nat. Mater.* **2012**, *11*, 432–435. [CrossRef] [PubMed]

199. Scherrer, S.; Scherrer, H.; Rowe, D. Bismuth Telluride, Antimony Telluride, and Their Solid Solutions. In *CRC Handbook of Thermoelectrics*; CRC Press: Boca Raton, FL, USA, 1995.

200. Sharp, J.W.; Sales, B.C.; Mandrus, D.G.; Chakoumakos, B.C. Thermoelectric Properties of Tl$_2$SnTe$_5$ and Tl$_2$GeTe$_5$. *Appl. Phys. Lett.* **1999**, *74*, 3794–3796. [CrossRef]

201. Skrabek, E.; Trimmer, D.; Rowe, D. Properties of the General TAGS System. In *CRC Handbook of Thermoelectrics*; CRC Press: Boca Raton, FL, USA, 1995.

202. Wan, C.; Wang, Y.; Wang, N.; Koumoto, K. Low-Thermal-Conductivity (MS)$_{1+x}$(TiS$_2$)$_2$ (M = Pb, Bi, Sn) Misfit Layer Compounds for Bulk Thermoelectric Materials. *Materials* **2010**, *3*, 2606–2617. [CrossRef]

203. Wang, W.H. Metallic Glasses: Family Traits. *Nat. Mater.* **2012**, *11*, 275–276. [CrossRef]

204. Warren, S.C.; Perkins, M.R.; Adams, A.M.; Kamperman, M.; Burns, A.A.; Arora, H.; Herz, E.; Suteewong, T.; Sai, H.; Li, Z.; et al. A Silica Sol-Gel Design Strategy for Nanostructured Metallic Materials. *Nat. Mater.* **2012**, *11*, 460–467. [CrossRef]

205. Cui, J.L.; Xue, H.F.; Xiu, W.J. Preparation and Thermoelectric Properties of P-Type $(Ga_2Te_3)x–(Bi_{0.5}Sb_{1.5}Te_3)_{1-x}$ (X = 0–0.2) Alloys Prepared by Spark Plasma Sintering. *Intermetallics* **2007**, *15*, 1466–1470. [CrossRef]

206. Gayner, C.; Nandihalli, N. Enhancement of Thermoelectric Performance of PbTe by Embedding NaCl. *Materialia* **2020**, *14*, 100912. [CrossRef]

207. Chang, C.-C.; Liu, C.-H.; Wu, C.-C.; Bag, P.; Kuo, Y.-K. Thermoelectric Properties of $(HgTe)_{0.55}(PbTe)_{0.45}$ Eutectic Composite with In Doping. *Mater. Res. Bull.* **2020**, *129*, 110916. [CrossRef]

208. Nandihalli, N.; Pai, Y.-H.; Liu, C.-J. Thermoelectric Properties of $Pb_{0.833}Na_{0.017}(Zn_{0.85}Al_{0.15})_{0.15}Te$-Te Composite. *Ceram. Int.* **2020**, *46*, 18683–18689. [CrossRef]

209. Zhu, C.; Zhang, J.; Ming, H.; Lou, X.; Huang, L.; Chen, T.; Zhang, B.; Li, D.; Xin, H.; Qin, X. Enhanced Thermoelectric Performance of PbTe Based Materials by Bi Doping and Introducing MgO Nanoparticles. *Appl. Phys. Lett.* **2020**, *117*, 042105. [CrossRef]

210. Yang, Z.-R.; Liu, C.-J. Thermoelectric Transport in P-Type $(Pb_{0.98}Na_{0.02}Te)_{1-x}(Zn_{0.85}Al_{0.15}Te)_x$-Te Composites Fabricated Using a Combination of Hydrothermal Synthesis and Evacuating-and-Encapsulating Sintering. *J. Electron. Mater.* **2020**, *49*, 2954–2961. [CrossRef]

211. Zhu, T.; Xie, H.; Zhang, C.; Cheng, X.; Zhang, J.; Poudeu, P.F.P.; Tan, G.; Yan, Y.; Liu, W.; Su, X.; et al. Enhanced Mechanical Properties of $Na_{0.02}Pb_{0.98}Te/MoTe_2$ Thermoelectric Composites Through in-Situ-Formed $MoTe_2$. *ACS Appl. Mater. Interfaces* **2019**, *11*, 41472–41481. [CrossRef]

212. Gao, J.; Mao, T.; Lv, T.; Li, Z.; Xu, G. Thermoelectric Performance of N-Type $(PbTe)_{1-x}(CoTe)_x$ Composite Prepared by High Pressure Sintering Method. *J. Mater. Sci. Mater. Electron.* **2018**, *29*, 5327–5336. [CrossRef]

213. Ginting, D.; Lin, C.-C.; Rathnam, L.; Hwang, J.; Kim, W.; Al Orabi, R.A.r.; Rhyee, J.-S. Dataset on the Electronic and Thermal Transport Properties of Quaternary Compounds of $(PbTe)_{0.95-x}(PbSe)_x(PbS)_{0.05}$. *Data Brief* **2017**, *13*, 233–241. [CrossRef] [PubMed]

214. Rösch, A.G.; Giunta, F.; Mallick, M.M.; Franke, L.; Gall, A.; Aghassi-Hagmann, J.; Schmalian, J.; Lemmer, U. Improved Electrical, Thermal, and Thermoelectric Properties Through Sample-to-Sample Fluctuations in Near-Percolation Threshold Composite Materials. *Adv. Simul.* **2021**, *4*, 2000284. [CrossRef]

215. Bruggeman, D.A.G. Berechnung Verschiedener Physikalischer Konstanten von Heterogenen Substanzen. I. Dielektrizitätskonstanten Und Leitfähigkeiten Der Mischkörper Aus Isotropen Substanzen. *Ann. Physik* **1935**, *416*, 636–664. [CrossRef]

216. Landauer, R. The Electrical Resistance of Binary Metallic Mixtures. *J. Appl. Phys.* **1952**, *23*, 779–784. [CrossRef]

217. Vaney, J.B.; Piarristeguy, A.; Ohorodniichuck, V.; Ferry, O.; Pradel, A.; Alleno, E.; Monnier, J.; Lopes, E.B.; Goncalves, A.P.; Delaizir, G.; et al. Effective Medium Theory Based Modeling of the Thermoelectric Properties of Composites: Comparison between Predictions and Experiments in the Glass-Crystal Composite System $Si_{10}As_{15}Te_{75}$-$Bi_{0.4}Sb_{1.6}Te_3$. *J. Mater. Chem. C* **2015**, *3*, 11090–11098. [CrossRef]

218. Sonntag, J. Comment on Effective Medium Theory Based Modeling of the Thermoelectric Properties of Composites: Comparison between Predictions and Experiments in the Glass–Crystal Composite System $Si_{10}As_{15}Te_{75}$-$Bi_{0.4}Sb_{1.6}Te_3$ by J.-B. Vaney et al., J. Mater. Chem. C, **2015**, *3*, 11090. *J. Mater. Chem. C* **2016**, *4*, 10973–10976. [CrossRef]

219. Angst, S.; Wolf, D.E. Network Theory for Inhomogeneous Thermoelectrics. *New J. Phys.* **2016**, *18*, 043004. [CrossRef]

220. Gather, F.; Heiliger, C.; Klar, P.J. NeMo: A Network Model Program for Analyzing the Thermoelectric Properties of Meso and Nanostructured Composite Materials. *Prog. Solid State Chem.* **2011**, *39*, 97–107. [CrossRef]

221. Aboudi, J.; Haj-Ali, R. A Fully Coupled Thermal–Electrical–Mechanical Micromodel for Multi-Phase Periodic Thermoelectrical Composite Materials and Devices. *Int. J. Solids Struct.* **2016**, *80*, 84–95. [CrossRef]

222. Monticelli, A. *State Estimation in Electric Power Systems: A Generalized Approach*, 1st ed.; Springer Science & Business Media: Berlin/Heidelberg, Germany, 1999.

223. Razavi, B. *Fundamentals of Microelectronics*, 2nd ed.; Wiley: Hoboken, NJ, USA, 2013; ISBN 978-1-118-15632-2.

224. Roche, S. Graphene Gets a Better Gap. *Nat. Nanotechnol.* **2010**, *6*, 8–9. [CrossRef]

225. Suh, D.; Lee, S.; Mun, H.; Park, S.H.; Lee, K.H.; Kim, S.W.; Choi, J.Y.; Baik, S. Enhanced Thermoelectric Performance of Bi0.5Sb1.5Te3-Expanded Graphene Composites by Simultaneous Modulation of Electronic and Thermal Carrier Transport. *Nano Energy* **2015**, *13*, 67–76. [CrossRef]

226. Yadav, S.; Chaudhary, S.; Pandya, D.K. Effect of 2D MoS_2 and Graphene Interfaces with $CoSb_3$ Nanoparticles in Enhancing Thermoelectric Properties of 2D MoS_2-$CoSb_3$ and Graphene-$CoSb_3$ Nanocomposites. *Ceram. Int.* **2018**, *44*, 10628–10634. [CrossRef]

227. Zhang, Y.; Ma, H.; Sun, B.; Liu, B.; Liu, H.; Kong, L.; Liu, B.; Jia, X.; Chen, X. Thermoelectric Performance of Graphene Composited BiSbTe Bulks by High Pressure Synthesis. *J. Alloys Compd.* **2017**, *715*, 344–348. [CrossRef]

228. He, Y.; Zhang, T.S.; Shi, X.; Wei, S.H.; Chen, L.D. High Thermoelectric Performance in Copper Telluride. *NPG Asia Mater.* **2015**, *7*, e210. [CrossRef]

229. Sottmann, J.; Valset, K.; Karlsen, O.B.; Tafto, J. Synthesis and Measurement of the Thermoelectric Properties of Multiphase Composites: ZnSb Matrix with Zn_4Sb_3, Zn_3P_2, and Cu_5Zn_8. *J. Electron. Mater.* **2013**, *42*, 1820–1826. [CrossRef]

230. Yamini, S.A.; Brewis, M.; Byrnes, J.; Santos, R.; Manettas, A.; Pei, Y.Z. Fabrication of Thermoelectric Materials—Thermal Stability and Repeatability of Achieved Efficiencies. *J. Mater. Chem. C* **2015**, *3*, 10610–10615. [CrossRef]

231. Aminorroaya Yamini, S.; Mitchell, D.R.G.; Wang, H.; Gibbs, Z.M.; Pei, Y.; Dou, S.X.; Snyder, G.J. Origin of Resistivity Anomaly in P-Type Leads Chalcogenide Multiphase Compounds. *AIP Adv.* **2015**, *5*, 053601. [CrossRef]

232. Shen, J.J.; Hu, L.P.; Zhu, T.J.; Zhao, X.B. The Texture Related Anisotropy of Thermoelectric Properties in Bismuth Telluride Based Polycrystalline Alloys. *Appl. Phys. Lett.* **2011**, *99*, 124102. [CrossRef]

233. Zhao, X.B.; Ji, X.H.; Zhang, Y.H.; Zhu, T.J.; Tu, J.P.; Zhang, X.B. Bismuth Telluride Nanotubes and the Effects on the Thermoelectric Properties of Nanotube-Containing Nanocomposites. *Appl. Phys. Lett.* **2005**, *86*, 062111. [CrossRef]

234. Bailyn, M. Maximum Variational Principle for Conduction Problems in a Magnetic Field, and the Theory of Magnon Drag. *Phys. Rev.* **1962**, *126*, 2040–2054. [CrossRef]

235. Hirohata, A.; Yamada, K.; Nakatani, Y.; Prejbeanu, I.L.; Dieny, B.; Pirro, P.; Hillebrands, B. Review on Spintronics: Principles and Device Applications. *J. Magn. Magn. Mater.* **2020**, *509*, 166711. [CrossRef]

236. Costache, M.V.; Bridoux, G.; Neumann, I.; Valenzuela, S.O. Magnon-Drag Thermopile. *Nat. Mater.* **2011**, *11*, 199–202. [CrossRef]

237. Watzman, S.J.; Duine, R.A.; Tserkovnyak, Y.; Boona, S.R.; Jin, H.; Prakash, A.; Zheng, Y.H.; Heremans, J.P. Magnon-Drag Thermopower and Nernst Coefficient in Fe, Co, and Ni. *Phys. Rev. B* **2016**, *94*, 144407. [CrossRef]

238. Saito, T.; Nishio-Hamane, D. Magnetic and Thermoelectric Properties of Co_2MnT (T = Ga, Si) Heusler Compounds. *Phys. B Condens. Matter* **2021**, *603*. [CrossRef]

239. Saito, T.; Kamishima, S. Magnetic and Thermoelectric Properties of Fe–Ti–Sn Alloys. *IEEE Trans. Magn.* **2019**, *55*, 2900104. [CrossRef]

240. Vikram, F.; Johnson, D.D.; Alam, A. Enhanced Thermoelectric Performance of $Mg_2Si_{1-x}Sn_x$ Codoped with Bi and Cr. *Phys. Rev. B* **2018**, *98*, 115204. [CrossRef]

241. Solomon, G.; Song, E.; Gayner, C.; Martinez, J.A.; Amouyal, Y. Effects of Microstructure and Neodymium Doping on Bi_2Te_3 Nanostructures: Implications for Thermoelectric Performance. *ACS Appl. Nano Mater.* **2021**, *4*, 4419–4431. [CrossRef]

242. Jena, A.; Lee, S.-C.; Bhattacharjee, S. Tuning the Lattice Thermal Conductivity in Bismuth Telluride via Cr Alloying. *Phys. Rev. Appl.* **2021**, *15*, 064023. [CrossRef]

243. Das, S.; Valiyaveettil, S.M.; Chen, K.-H.; Suwas, S.; Mallik, R.C. Thermoelectric Properties of Mn Doped BiCuSeO. *Mater. Res. Express* **2019**, *6*, 086305. [CrossRef]

244. Diakhate, M.S.; Hermann, R.P.; Mochel, A.; Sergueev, I.; Sondergaard, M.; Christensen, M.; Verstraete, M.J. Thermodynamic, Thermoelectric, and Magnetic Properties of $FeSb_2$: A Combined First-Principles and Experimental Study. *Phys. Rev. B* **2011**, *84*, 125210. [CrossRef]

245. Sun, P.; Oeschler, N.; Johnsen, S.; Iversen, B.B.; Steglich, F. Narrow Band Gap and Enhanced Thermoelectricity in $FeSb_2$. *Dalton Trans.* **2010**, *39*, 1012–1019. [CrossRef] [PubMed]

246. Franzen, H.; Sterner, C. The X-Ray Photoelectron Spectra of MnS, MnSe, and MnTe. *J. Solid State Chem.* **1978**, *25*, 227–230. [CrossRef]

247. Podgorny, M.; Oleszkiewicz, J. Electronic Structure of Antiferromagnetic MnTe. *J. Phys. C Solid State Phys.* **1983**, *16*, 2547–2557. [CrossRef]

248. Wasscher, J.D.; Haas, C. Contribution of Magnon-Drag to the Thermoelectric Power of Antiferromagnetic Mn Te. *Phys. Lett.* **1964**, *8*, 302–304. [CrossRef]

249. Peng, C.; Zhang, G.; Wang, C.; Yan, Y.; Zheng, H.; Wang, Y.; Hu, M. Improvement of Thermoelectricity Through Magnetic Interactions in Layered $Cr_2Ge_2Te_6$. *Phys. Status Solidi RRL Rapid Res. Lett.* **2018**, *12*, 1800172. [CrossRef]

250. Kirkham, M.J.; dos Santos, A.M.; Rawn, C.J.; Lara-Curzio, E.; Sharp, J.W.; Thompson, A.J. Abinitio Determination of Crystal Structures of the Thermoelectric Material MgAgSb. *Phys. Rev. B* **2012**, *85*, 144120. [CrossRef]

251. Zheng, L.; Li, J.; Zhou, B.; Liu, H.; Bu, Z.; Chen, B.; Ang, R.; Li, W. Thermoelectric Properties of P-Type MnSe. *J. Alloys Compd.* **2019**, *789*, 953–959. [CrossRef]

252. Shimizu, S.; Shiogai, J.; Takemori, N.; Sakai, S.; Ikeda, H.; Arita, R.; Nojima, T.; Tsukazaki, A.; Iwasa, Y. Giant Thermoelectric Power Factor in Ultrathin FeSe Superconductor. *Nat. Commun.* **2019**, *10*, 825. [CrossRef]

253. Takahashi, H.; Okazaki, R.; Ishiwata, S.; Taniguchi, H.; Okutani, A.; Hagiwara, M.; Terasaki, I. Colossal Seebeck Effect Enhanced by Quasi-Ballistic Phonons Dragging Massive Electrons in $FeSb_2$. *Nat. Commun.* **2016**, *7*, 12732. [CrossRef]

254. Tsujii, N.; Mori, T. High Thermoelectric Power Factor in a Carrier-Doped Magnetic Semiconductor $CuFeS_2$. *Appl. Phys. Express* **2013**, *6*, 043001. [CrossRef]

255. Ang, R.; Khan, A.U.; Tsujii, N.; Takai, K.; Nakamura, R.; Mori, T. Thermoelectricity Generation and Electron-Magnon Scattering in a Natural Chalcopyrite Mineral from a Deep-Sea Hydrothermal Vent. *Angew. Chem. Int. Ed. Engl.* **2015**, *54*, 12909–12913. [CrossRef]

256. Kikkawa, T.; Reitz, D.; Ito, H.; Makiuchi, T.; Sugimoto, T.; Tsunekawa, K.; Daimon, S.; Oyanagi, K.; Ramos, R.; Takahashi, S.; et al. Observation of Nuclear-Spin Seebeck Effect. *Nat. Commun.* **2021**, *12*, 4356. [CrossRef] [PubMed]

257. Uchida, K.; Takahashi, S.; Harii, K.; Ieda, J.; Koshibae, W.; Ando, K.; Maekawa, S.; Saitoh, E. Observation of the Spin Seebeck Effect. *Nature* **2008**, *455*, 778–781. [CrossRef] [PubMed]

258. Wang, Y.; Rogado, N.S.; Cava, R.J.; Ong, N.P. Spin Entropy as the Likely Source of Enhanced Thermopower in $Na(x)Co_2O_4$. *Nature* **2003**, *423*, 425–428. [CrossRef]

259. Bauer, G.E.; Saitoh, E.; van Wees, B.J. Spin Caloritronics. *Nat. Mater.* **2012**, *11*, 391–399. [CrossRef] [PubMed]

260. Yu, H.M.; Brechet, S.D.; Ansermet, J.P. Spin Caloritronics, Origin and Outlook. *Phys. Lett. A* **2017**, *381*, 825–837. [CrossRef]

261. Erekhinsky, M.; Casanova, F.; Schuller, I.K.; Sharoni, A. Spin-Dependent Seebeck Effect in Non-Local Spin Valve Devices. *Appl. Phys. Lett.* **2012**, *100*, 212401. [CrossRef]

262. Marchal, N.; da Camara Santa Clara Gomes, T.; Abreu Araujo, F.; Piraux, L. Large Spin-Dependent Thermoelectric Effects in NiFe-Based Interconnected Nanowire Networks. *Nanoscale Res. Lett.* **2020**, *15*, 137. [CrossRef]

263. Yamanoi, K.; Yafuso, M.; Miyazaki, K.; Kimura, T. Signature of Spin-Dependent Seebeck Effect in Dynamical Spin Injection of Metallic Bilayer Structures. *J. Phys. Mater.* **2019**, *3*, 014005. [CrossRef]

264. Ahmed, F.; Tsujii, N.; Mori, T. Thermoelectric Properties of $CuGa_{1-x}Mn_xTe_2$: Power Factor Enhancement by Incorporation of Magnetic Ions. *J. Mater. Chem. A* **2017**, *5*, 7545–7554. [CrossRef]

265. Vaney, J.B.; Yamini, S.A.; Takaki, H.; Kobayashi, K.; Kobayashi, N.; Mori, T. Magnetism-Mediated Thermoelectric Performance of the Cr-Doped Bismuth Telluride Tetradymite. *Mater. Today Phys.* **2019**, *9*, 100090. [CrossRef]

266. Acharya, S.; Anwar, S.; Mori, T.; Soni, A. Coupling of Charge Carriers with Magnetic Entropy for Power Factor Enhancement in Mn Doped $Sn_{1.03}Te$ for Thermoelectric Applications. *J. Mater. Chem. C* **2018**, *6*, 6489–6493. [CrossRef]

267. Li, W.; Chen, Z.W.; Lin, S.Q.; Chang, Y.J.; Ge, B.H.; Chen, Y.; Pei, Y.Z. Band and Scattering Tuning for High Performance Thermoelectric $Sn_{1-x}Mn_xTe$ Alloys. *J. Mater.* **2015**, *1*, 307–315. [CrossRef]

268. He, J.; Tan, X.; Xu, J.; Liu, G.-Q.; Shao, H.; Fu, Y.; Wang, X.; Liu, Z.; Xu, J.; Jiang, H.; et al. Valence Band Engineering and Thermoelectric Performance Optimization in SnTe by Mn-Alloying via a Zone-Melting Method. *J. Mater. Chem. A* **2015**, *3*, 19974–19979. [CrossRef]

269. Graf, T.; Barth, J.; Blum, C.G.F.; Balke, B.; Felser, C.; Klaer, P.; Elmers, H.-J. Phase-Separation-Induced Changes in the Magnetic and Transport Properties of the Quaternary Heusler Alloy $Co_2Mn_{1-x}Ti_xSn$. *Phys. Rev. B* **2010**, *82*, 104420. [CrossRef]

270. Liu, Z.; Zhu, J.; Wei, P.; Zhu, W.; Zhao, W.; Xia, A.; Xu, D.; Lei, Y.; Yu, J. Candidate for Magnetic Doping Agent and High-Temperature Thermoelectric Performance Enhancer: Hard Magnetic M-Type $BaFe_{12}O_{19}$ Nanometer Suspension. *ACS Appl. Mater. Interfaces* **2019**, *11*, 45875–45884. [CrossRef]

271. Zhao, W.; Liu, Z.; Wei, P.; Zhang, Q.; Zhu, W.; Su, X.; Tang, X.; Yang, J.; Liu, Y.; Shi, J.; et al. Magnetoelectric Interaction and Transport Behaviours in Magnetic Nanocomposite Thermoelectric Materials. *Nat. Nanotechnol.* **2017**, *12*, 55–60. [CrossRef]

272. Lu, R.; Lopez, J.S.; Liu, Y.; Bailey, T.P.; Page, A.A.; Wang, S.; Uher, C.; Poudeu, P.F.P. Coherent Magnetic Nanoinclusions Induce Charge Localization in Half-Heusler Alloys Leading to High-Tc Ferromagnetism and Enhanced Thermoelectric Performance. *J. Mater. Chem. A* **2019**, *7*, 11095–11103. [CrossRef]

273. Vandendriessche, S.; Brullot, W.; Slavov, D.; Valev, V.K.; Verbiest, T. Magneto-Optical Harmonic Susceptometry of Superparamagnetic Materials. *Appl. Phys. Lett.* **2013**, *102*, 161903. [CrossRef]

274. Marghussian, V. Magnetic Properties of Nano-Glass Ceramics. In *Nano-Glass Ceramics*; Elsevier: Amsterdam, The Netherlands, 2015; pp. 181–223, ISBN 978-0-323-35386-1.

275. Zhao, W.; Liu, Z.; Sun, Z.; Zhang, Q.; Wei, P.; Mu, X.; Zhou, H.; Li, C.; Ma, S.; He, D.; et al. Superparamagnetic Enhancement of Thermoelectric Performance. *Nature* **2017**, *549*, 247–251. [CrossRef] [PubMed]